NISTIR 6531

FLAMMABILITY OF POLYMER CLAY NANOCOMPOSITES CONSORTIUM: YEAR ONE ANNUAL REPORT

Jeffrey W. Gilman, Takashi Kashiwagi, Alexander B. Morgan, Richard H. Harris, Jr., Lori Brassell, Mark VanLandingham and Catheryn L. Jackson

United States Department of Commerce
Technology Administration
National Institute of Standards and Technology

NISTIR 6531

FLAMMABILITY OF POLYMER CLAY NANOCOMPOSITES CONSORTIUM: YEAR ONE ANNUAL REPORT

Jeffrey W. Gilman[1], Takashi Kashiwagi[1], Alexander B. Morgan[1], Richard H. Harris, Jr.[1], Lori Brassell[1], Mark VanLandingham[1] and Catheryn L. Jackson[2]
1-Building and Fire Research Laboratory, 2-Materials Science and Engineering Laboratory
National Institute of Standards and Technology
Gaithersburg, MD

July 2000

U.S. Department of Commerce
William M. Daley, *Secretary*
Technology Administration
Dr. Cheryl L. Shavers, *Under Secretary for Technology*
National Institute of Standards and Technology
Raymond G. Kammer, *Director*

List of Tables

List of Figures

Flammability of Polymer Clay Nanocomposites Consortium: Year One Annual Report

Consortium Manager: Jeffrey Gilman (NIST)

Consortium Team Members : Takashi Kashiwagi, Alexander Morgan, Richard Harris, Lori Brassell, Catheryn Jackson, Mark VanLandingham (NIST), Shawn Phillips (AFRL), Richard Lyon (FAA), John Campbell (GE), Barbara Stahly, Phil Chou, Leonard Chyall (Great Lakes Chemical), William Schultz (3M), Gary Beall (Nanocor), John Lau (PQ), Hiro Kato, Koichi Shibayama (Sekisui)

Douglas Hunter (Southern Clay Products), Ali Firouzi (Raychem/Tyco Electronics).

Executive Summary

We recently found that polymer layered-silicate (clay) nanocomposites have the unique combination of reduced flammability and improved physical properties. However, the details of the fire retardant mechanism were not well understood. In October of 1998 a NIST-industrial consortium was formed to study the flammability of these unique materials.

During the first year our goals were to compare the flammability properties of:

1) intercalated versus delaminated nanocomposites,
2) tethered versus non-tethered nanocomposites,
3) nanocomposites with different layered silicates (clays),
4) nanocomposites crosslinked to different degrees,
5) nanocomposites with different melt viscosities,
6) nanocomposites with different silicate loading levels, and
7) nanocomposites incorporating a charring-resin, polyphenyleneoxide (PPO), into a blend.

The most important result from our first year's work is the discovery that a clay-reinforced carbonaceous char forms during combustion of nanocomposites. This is particularly significant for systems whose base resin normally produces little or no char when burned alone (PS, PPgMA, PA-6 and EVA). It appears from the gasification data (videos and mass loss data) that this clay-reinforced carbonaceous char is responsible for the reduced mass loss rates, and hence the lower flammability.

Furthermore, we conclude that intercalated nanocomposites perform as well as delaminated nanocomposites. We were not able to determine if there is an effect of tethering, due to the weak effect observed for the epoxy nanocomposites. We did not explore nanocomposites with different layered silicates (clays). We believe that a small but significant effect on flammability may be due to the greater melt viscosity of the nanocomposites, but rheological measurements still need to be made to confirm this hypothesis. In terms of the effect of loading level, the effectiveness of the nanocomposite approach to reducing flammability, in most cases, levels off at a mass fraction of 5 % silicate loading. And finally, the use of a char-enhancer (PPO) did not decrease the flammability of the PA-6 nanocomposites, but other char-enhancing co-additives should be explored.

1. Introduction

In 1997 NIST reported that polymer layered-silicate (clay) nanocomposites exhibit reduced flammability and improved physical properties at low cost[1]. However, the details of the fire retardant mechanism were not well understood. In October of 1998 a NIST-industrial consortium was formed to study the flammability of these unique materials. This report covers the research results from the first year of this program.

1.1 Goals for Year One

The focus of research within this consortium is on the development of a fundamental understanding of the fire retardant (FR) mechanism of polymer clay nanocomposites. The goals for Year One of the consortium were to determine the effects of varying specific nano-structural parameters on the flammability of polymer clay nanocomposites. These goals were as follows: To compare the flammability properties of: 1) intercalated versus delaminated nanocomposites, 2) tethered versus non-tethered nanocomposites, 3) nanocomposites with different layered silicates (clays), i.e., hectorite versus montmorillonite, 4) nanocomposites crosslinked to different degrees, 5) nanocomposites with different melt viscosities, 6) nanocomposites with different silicate loading levels, and 7) nanocomposites incorporating a charring-resin, polyphenyleneoxide (PPO), into a blend.

The outline below shows these parameters and the specific approach we planned to use to investigate each parameter. Several resin systems will be used for these studies. Polypropylene (PP), polystyrene (PS), poly(ethylene vinyl acetate) copolymer (EVA), polyamide-6 (PA-6) and epoxy thermosets based on the diglycidylether of bis-phenol-A (DGEBA).

1.2 Nanocomposite Parameters and Critical Experiments Outline: [¥]

1. Intercalated vs. delaminated:

A. PA-6 Nanocomposite System: GE will prepare intercalated and delaminated PA-6 montmorillonite clay (MMT, 5 %[*]) nanocomposites via melt blending.

B. PP Nanocomposite System: Sekisui will prepare intercalated and delaminated PP clay (MMT, 5 %) nanocomposites via melt blending using PP-g-MA.

2. Tethered vs. non-tethered:

A. PA-6 Nanocomposite System : GE will prepare delaminated PA-6 clay (MMT, 5 %) nanocomposites via melt blending (non-tethered) for comparison to commercially available delaminated PA-6 clay (MMT, 5 %) nanocomposites made via *in situ* polymerization (tethered).

[¥] The policy of the National Institute of Standards and Technology (NIST) is to use metric units of measurement in all its publications, and to provide statements of uncertainty for all original measurements. In this document however, data from organizations outside NIST are shown, which may include measurements in non-metric units or measurements without uncertainty statements.

The identification of any commercial product or trade name does not imply endorsement or recommendation by the National Institute of Standards and Technology.

[*] Throughout this paper, whenever % is used to refer to the amount of silicate (clay) loading in a polymer nanocomposite, it refers to a mass fraction of that %, unless stated otherwise.

B. Epoxy Nanocomposite System : 3M will prepare delaminated epoxy clay (MMT, 5 %) nanocomposites using different organic treatments on the MMT clay to give a tethered and a non-tethered version.

3. Type of Clay :

A. PA-6 Nanocomposite System: GE will prepare several delaminated PA-6 clay (5 %) nanocomposites via melt blending using MMT, laponite and hectorite.

B. Epoxy Nanocomposite System : 3M will prepare delaminated epoxy clay (5 %) nanocomposites using MMT, laponite and hectorite.

4. Effect of Crosslinking :

A. PE Nanocomposite System: Raychem will prepare delaminated PE clay (MMT, 5 %) nanocomposites via melt blending (using PE-g-MA) with a subsequent e-beam exposure to give 3 different levels of crosslinking.

5. Polymer Molecular Mass :

A. PS Nanocomposite System: Great Lakes Chemical will prepare intercalated PS clay (MMT, 2 %, 5 % , 10 %) nanocomposites using two different Mw of PS.

6. Effect of Loading :

A. PA-6 Nanocomposite System: GE will prepare delaminated PA-6 clay (MMT, 2 %, 5 %, and 10 %) nanocomposites via melt blending.

B. PP Nanocomposite System: Sekisui will prepare intercalated PP clay (MMT, 2 %, 5 % and 10 %) nanocomposites via melt blending using PP-g-MA.

C. PS Nanocomposite System: Great Lakes Chemical will prepare intercalated PS clay (MMT, 2 %, 5 % and 10 %) nanocomposites using 2 different Mw of PS.

7. Effect of Charring Agents :

A. PA-6 Nanocomposite System : GE will prepare delaminated PA-6/PPO clay (MMT, 5 %) nanocomposites via melt blending.

2. Experimental

2.1 Processing

In general, the thermoplastic resins (PP, PE (EVA), PS and PA-6) used to prepare the nanocomposites were compounded via melt blending in a twin-screw extruder[2]. PA-6 clay nanocomposites were also prepared via the *in situ* process developed by Unitika[3] and Toyota[4]. The *in situ* prepared PA-6 materials were obtained from UBE Inc. The epoxy nanocomposites were made by standard techniques shown below. In regards to the exact nature of these polymer nanocomposite formulations, we are uncertain about the exact amount of clay loading or of co-additive used, as these samples were prepared outside of NIST. One group of samples (EVA Nanocomposites) were analyzed (by Raychem) for actual clay loadings, although no error analysis was done for this analysis.

2.1.1. PA-6 Nanocomposites.

PA6 nanocomposites were compounded by GE on a twin screw extruder (Welding Engineer, non-intermeshing, counter-rotating, die and 4 barrel segments at 246 °C, 41.88 rad/s [400 rpm], feed rate 6 kg/h). PA-6 (Capron C1250) powder was mixed with organic treated montmorillonite (Southern Clay Products, SCPX 2173, quaternary alkyl ammonium MMT) to prevent segregation, and was then combined with PA-6 pellets in the extruder. Polyphenyleneoxide (PPO) was blended with two of the formulations. The formulations are shown in Table 1.

Table 1. PA-6 nanocomposite formulations.

PA-6 (powder, %)	PA-6 (pellets, %)	Clay (%)	PPO (%)
74	24	2	0
72	23	5	0
70	20	10	0
62	28	4.75	5
65	20	4.5	10

Clay- SCPX 2173; % is mass fraction %

2.1.2. EVA-Nanocomposites.

Poly (ethylene vinyl acetate) (EVA, Elvax-460, mass fraction VA 18 %) was compounded by Raychem on a twin screw extruder (Leistritz, micro 27, co-rotating, 27 mm screw diameter, L/D ratio: 40, zone temperatures: 90 °C to130 °C, screw speed: 42 rad/s to 52 rad/s [RPM: 400 to 500], barrel pressures: 4830 kPa to 8720 kPa [700 psi to1200 psi], melt temperatures: 215 °C to 235 °C). The EVA was compounded with organic treated montmorillonite, one from Southern Clay Products, SCPX 2156, a quaternary alkyl ammonium treated MMT, and two from Nanocor, 1.30E, an octadecyl ammonium treated MMT, and 1.30D, a dodecyl pyrrolidone treated MMT. Variation in crosslink density was introduced by exposing the EVA/MMT nanocomposites to electron beam irradiation (beam dosage: 25 kGy, 39 kGy, and 64 kGy [2.5 MRad, 3.9 MRad and 6.4 MRad] respectively).

Table 2. EVA nanocomposite formulations

Clay type	Clay Supplier	Type of Treatment	Clay treatment	Organic Fraction	Desired Clay Loading [%]	Actual Clay Loading [%]
SCPX 2156	SCP	Onium	Quat. Alkyl Ammon.	0.39	2	2.1
SCPX 2156	SCP	Onium	Quat. Alkyl Ammon.	0.39	5	6.7
SCPX 2156	SCP	Onium	Quat. Alkyl Ammon.	0.39	10	9.7
I.30 E	Nanocor	Onium	Protonated ODA	0.35	2	2.2
I.30 E	Nanocor	Onium	Protonated ODA	0.35	5	6.4
I.30 D	Nanocor	Ion-dipole	DDP	0.36	2	2.1

ODA: Octadecyl Amine, DDP: Dodecylpyrrolidone, Organic fraction determined by TGA (1000 °C)
Actual clay loading determined by measuring the "ash" percentage in a tube furnace

2.1.3. PP-Nanocomposites.

Polypropylene(PP)-nanocomposites were compounded by Sekisui on a twin-screw extruder (JSW, TEX30 alpha, 32 mm screw diameter, co-rotating , L/D ratio: 51, zone temperatures: 170 °C to190 °C, die temperature 190 °C, feed rate 15 kg/h). PP (Mitsubishi Chemical, Novatech EA9, melt flow index: 0.5 g/ 10 min, d= 0.9 g/cm^3) was compounded with organic treated montmorillonite from Southern Clay Products (SCPX 1980, a quaternary alkyl ammonium MMT) and organic treated montmorillonite from Nanocor (ODA Nanomer, octadecyl ammonium MMT). Polypropylene-graft-maleic anhydride (PP-g-MA, Sanyo Kasei, acid number: 26 mg KOH/g, mole fraction MA = 0.9 %, Mw$^{\Psi}$: 40000, Tg 154 °C) was used as a compatibilizer for some of the formulations. The formulations prepared are shown in Table 3.

Table 3. PP formulations

PP (mass fraction %)	PP-g-MA (mass fraction %)	Clay (SCPX1980)	Clay (ODA Nanomer)
100	0	0	0
85	15	0	0
95	0	5	0
80	15	5	0
83	15	2	0
75	15	10	0
95	0	0	5
80	15	0	5
83	15	0	2
75	15	0	10

2.1.4. PS-Nanocomposites

PS-nanocomposites were prepared by Great Lakes Chemical. PS of two different Mw[5] (Mw 170,000, Styron 663 and Mw 100,000 XU70262.08) were compounded with organic treated montmorillonite from Southern Clay Products (Cloisite 20A) using a Berstorff ZE-25 twin-screw extruder (L/D = 35) at 170 °C with a nominal screw speed of 20.9 rad/s [200 rpm]. The material was extruded at a rate of

$^{\Psi}$ All molecular masses (Mw) referred to throughout the paper are relative molecular masses. See refs 5 and 13.

250 g/min and the extruded strands were cooled in a water bath and pelletized with a Conair Jetro model # 3045/0-9478 pelletizer. The formulations prepared are shown in Table 4.

Table 4. PS formulations.

High Mw PS	Low Mw PS	Clay (SCPX2197)
98	-	2
95	-	5
90	-	10
-	98	2
-	95	5
-	90	10

2.1.5. Epoxy-Nanocomposites

Epoxy-nanocomposites were prepared by 3M. An aromatic amine cured epoxy nanocomposite was prepared using Epon 828 (Shell, mass fraction 79 % (100 parts)), Curative W (Figure 1, Shell, mass fraction 21 % (26.5 parts)) and organic treated montmorillonite from Southern Clay Products (SCPX 2003, a bis-2-hydroxyethyl alkyl ammonium MMT). An anhydride cured epoxy-nanocomposite was also prepared using Epon 828 (Shell, mass fraction 59 % (100 parts)), hexahydro-4-methylphthalic anhydride (mass fraction 40 % (68 parts)), benzyldimethyl amine (mass fraction 0.6 % (1 part)) and organic treated montmorillonite (SCPX 2165, a non-reactive, quaternary alkyl ammonium MMT). Clay addition was adjusted to a mass fraction of 5 % inorganic in the samples. Clay was mixed in at 80 °C for 1 h with a very high shear mixer. A Hegman gage was used to follow the dispersion. Samples were cured for 1 h at 100 °C, 1 h at 150 °C and 1 h at 175 °C.

Table 5. Epoxy formulations

Resin/curative	Clay
Epoxy/ anhydride	none
Epoxy/ anhydride (non-tethered)	SCPX 2165
Epoxy/ anhydride (tethered)	SCPX 2003
Epoxy/ Aromatic amine	none
Epoxy/ aromatic amine (non-tethered)	SCPX 2165

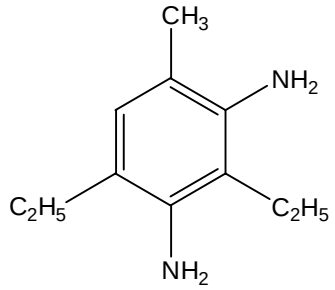

Figure 1. Aromatic amine, Curative W.

2.2. Injection Molding Procedure.

Disks, (7.5 cm diameter × 0.8 cm thick) for the Cone Calorimeter tests and two sizes of dog bones (ASTM D638 type IV and V) for mechanical property tests, were prepared using an injection molding machine (Gluco LP20B semiautomatic, pneumatic). The molding machine is rated at 18.1×10^3 kg (20 tons) with 690 kPa (100 psi) air pressure. The nozzle and melt chamber (barrel) will theoretically hold 62.4 g (2.2 ounces) of melt. All resins were dried at a time and temperature determined by the literature and kept in a desiccator over a desiccant until they were added to the injection molding machine.

The processing temperature was determined by the particular resin and the amount of injection pressure available. An effort was made to process the resins at as low a temperature and with as short a residence time as possible to avoid degradation. The resin shot was manually added to the barrel of the injection molding machine and packed into the melt chamber. Approximately one minute before the injection time, the resin was packed two more times for 10 s each. After each injection another shot was added to the barrel and the process repeated. A timer was used to determine when it was time to inject and filling of the barrel was done immediately after an injection to keep the residence time as equal as possible for each disk or set of dog bones. Table 6 summarizes the injection molding conditions for each of the resins supplied. Table 7 through Table 10 show the specific injection molding conditions for the individual polymers.

Table 6. Injection Molding Conditions for the Various Resins

Resin	Supplier	Shot Size (g)	Drying Time(s)@ Temp. (°C)	Processing Temp. (°C)	Residence Time (s)	Injection Pressure (kPa)
Nylon 6	General Electric	40.0	10800-@100	285	720-840	655-689
Polypropylene	Sekisui	32.0	7200-@80	200	600	689
Poly(ethylene vinyl acetate)	Raychem	33.5	7200-@55	107	600	552-655
Polystyrene	Great Lakes	38.0	7200-@70	200-225	600	689

Table 7. Injection Molding of Nylon 6

Clay Identity	Mass fraction % clay	Mass fraction % PPO	Process Temp. (°C)	Injection Pressure (kPa)
Blank	0	0	285	689
SCPX2173	2	0	285	689
SCPX2173	5	0	285	689
SCPX2173	10	0	285	655
SCPX2173	4.75	5	285	655
SCPX2173	4.5	10	285	655

Table 8. Injection Molding of Polypropylene

Clay Identity	Mass fraction % clay	Mass fraction % PP-g-MA	Process Temp. (°C)	Injection Pressure (kPa)
Blank	0	0	200	689
Blank	0	15	200	689
SCPX1980	5	0	200	689
SCPX1980	5	15	200	689
SCPX1980	2	15	200	689
SCPX1980	10	15	200	689
ODA Nanomer	5	0	200	689
ODA Nanomer	5	15	200	689
ODA Nanomer	2	15	200	689
ODA Nanomer	10	15	200	689

Table 9. Injection Molding of Ethylene Vinyl Acetate

Clay Identity	Mass fraction % Clay	Process Temp. (°C)	Injection Pressure (kPa)
Blank	0	107	552
SCPX2156	2	107	552
SCPX2156	5	107	655
SCPX2156	10	107	655
1.30 E	2	107	552
1.30 E	5	107	586
1.30 D	2	107	552
1.30 D	5	107	586

Table 10. Injection Molding of Polystyrene

Clay Identity	Mass fraction % Clay	Process Temp. (°C)	Injection Pressure (kPa)
Blank (low MW PS)	0	210	689
SCPX2197	2	210	689
SCPX2197	5	210	689
SCPX2197	10	210	689
Blank (high MW PS)	0	210	689
SCPX2197	2	225	689
SCPX2197	5	210	689
SCPX2197	10	200	689

2.2. Characterization

Each of the nanocomposite systems prepared was characterized using X-ray diffraction (XRD), and Transmission Electron Microscopy (TEM). In some cases additional analysis such as GPC and TGA were done also. Most TEM and XRD was done by the member that prepared the sample. The following TEM was performed at NIST.

TEM:
PS- nanocomposites:
TEM samples were prepared using room temperature ultramicrotomy to cut 70 nm thick sections. These sections were placed onto carbon-coated copper grids. Bright-field TEM images were obtained at 120 kV, at low dose conditions, with a Philips 400T at magnifications of 2800, 28000, and 60000×.

PE-nanocomposites:
TEM samples were prepared using cryo ultramicrotomy (-110 °C) to cut 70 nm thick sections. These sections were placed onto carbon-coated copper grids. Bright-field TEM images were obtained at 120 kV, at low dose conditions, with a Philips 400T at magnifications of 2800, 10000, 28000, and 60000×.

TEM negatives were then enlarged to 8400, 30000, 280000, and 600000× respectively to produce high magnification prints. The contrast between the layered silicates and the polymer phase was sufficient for imaging, so no heavy metal staining of sections prior to imaging was required.

XRD:
XRD data were collected on powder specimens (particle size of less than 40 μm) with a Philips diffractometer using Cu Kα radiation (λ=0.1505945 nm) with a 0.02 2θ step size and a 2 s count time.

In regards to the uncertainty of XRD measurements, some comments about the use of XRD when analyzing polymer-clay nanocomposites is needed.

While the peaks given by XRD measurements are traceable to the well-defined Cu Kα radiation do indeed refer to a well-known spacing between clay layers, the number given must be interpreted. A slight increase or decrease in spacing (± 5 %) is probably not significant, as the exact nature of the material between the clay layers (referred to as the gallery) is unknown. Material processing conditions, thermal stability of the organic treatment in the gallery, and the polymer itself can all affect the clay's d-spacing (distance between basal layers). Even at larger spacing increases or decreases, one cannot say definitely how much polymer has entered into the gallery, thus defining the amount of intercalation or delamination which occurred during the synthesis of the polymer-clay nanocomposite. XRD is a useful screening tool for determining if any sort of nanocomposite was prepared, but the results provided by XRD cannot be used alone to define the exact nature of the nanocomposite. XRD only gives the distance between clay layers, thus revealing the relationship of the clay layers to themselves, not of the clay layers to the polymer. XRD does not reveal how well dispersed the clay is throughout the polymer, nor does it define the degree of intercalation or exfoliation. Only TEM analysis can reveal this. Low magnification TEM will reveal how well dispersed the clay is throughout the polymer, and it can also show the degree of intercalation and exfoliation which occurred. Of final note, XRD results can be deceptive, suggesting that an intercalated material is well-dispersed, or that a material is an exfoliated nanocomposite, when in reality, the nanocomposite is neither well-dispersed or exfoliated.[6]

2.3. Cone Calorimetry

Cone Calorimeter experiments were performed at an incident heat flux of 50 kW/m^2[7]. Peak heat release rate (HRR), mass loss rate (MLR), specific extinction area (SEA), ignition time (t_{ign}), carbon monoxide yield, carbon dioxide yield, and specific heat of combustion data are reproducible to within ± 10 % when measured at 50 kW/m^2 flux. The cone data reported here are the average of three replicated experiments. The specific uncertainties (one sigma) are shown as error bars on the plots of the Cone data.

2.4. Gasification

The gasification device built at NIST is shown schematically in Figure 2. The cylindrical chamber is 0.61 m in diameter and 1.70 m in height. Two windows provide optical access. The chamber walls are water cooled to 25 °C. Products and ambient gases are removed via an exhaust duct, and a constant nitrogen flow of 7.67 L/s at 25 °C is maintained during the experiments. The temperature of the elements in the cone-shaped heater is fixed at 808 °C to maintain a constant emission spectrum for all tests. A water-cooled shutter was extended to protect the sample from the incident radiant flux during nitrogen purge, prior to testing. Flux levels varied about 8 % to 10 % across 0.1 m diameter sample region. The sample, 75 mm in diameter and 8 mm in thickness, was placed in an aluminum foil pan having nearly the same diameter as that of the sample, and 13 mm high side walls. The sample mass was measured by a load cell; these data were recorded at 0.5 s intervals. The gasification device allows pyrolysis, in a nitrogen atmosphere, of samples identical to those used in the Cone Calorimeter, without complications from gas phase combustion, such as heat feedback and obscuration of the sample surface by the flame. The uncertainty in the measurement of interest in the gasification data is shown in each plot as an error bar.

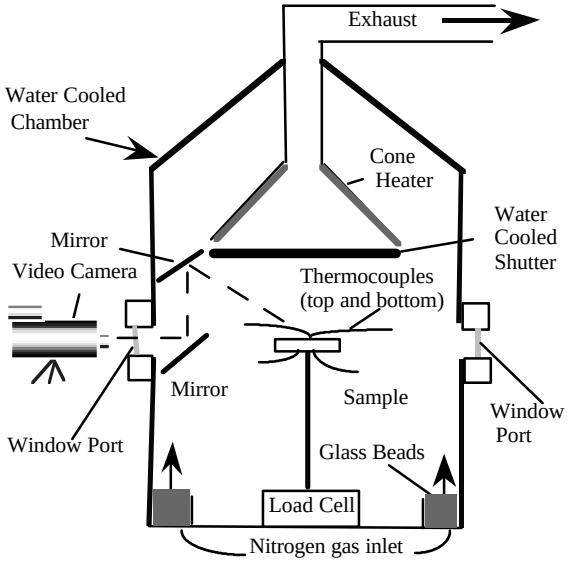

Figure 2. Schematic of Gasification device.

2.5. UL-94 Flammability Test[10]

The UL-94 test is performed on a plastic sample (125 mm by 13 mm, with various thicknesses up to 13mm) suspended vertically above a cotton patch. The plastic is subjected to two 10 s flame exposures with a calibrated flame in a unit which is free from the effects of external air currents. After the first 10 s exposure, the flame is removed, and the time for the sample to self-extinguish is recorded. Cotton ignition is noted if polymer dripping ensues; dripping is permissible if no cotton ignites. Then the second ignition is performed on the same sample, and the self-extinguishing time and dripping characteristics recorded. If the plastic self-extinguishes in less than 10 s after each ignition, with no dripping, it is classified as V-0. If it self-extinguishes in less than 30 s after each ignition, with no dripping, it is classified as a V-1, and if the cotton ignites then it is classified as V-2. If the sample does not self-extinguish before burning completely it is classified as failed (F).

3. Results and Discussion

3.1. PA-6 nanocomposites

The initial plans (also shown above in section 1.2) for PA-6 nanocomposites at the beginning of Year One included studying the effect of varying the following nanocomposite parameters (critical experiment number in parenthesis): (1) intercalated versus delaminated nanocomposites, (2) tethered versus non-tethered nanocomposites, (3) nanocomposites with different layered silicates (clays), i.e., hectorite versus montmorillonite, (6) nanocomposites with different silicate loading levels and (7) nanocomposites incorporating a charring-resin, polyphenyleneoxide (PPO), into a blend. As of the end of the first year, critical experiments 1, 6, and 7 have been addressed.

3.1.1. Characterization

The PA-6 nanocomposites were prepared with an intercalated nanomorphology by extruding the PA-6 with dimethyl, dihydrogenated-tallow ammonium treated montmorillonite. XRD analysis showed the

layer spacing to be 2.45 nm. TEM (Figure 3) shows tactoids with expanded d-spacings and confirms the intercalated structure.

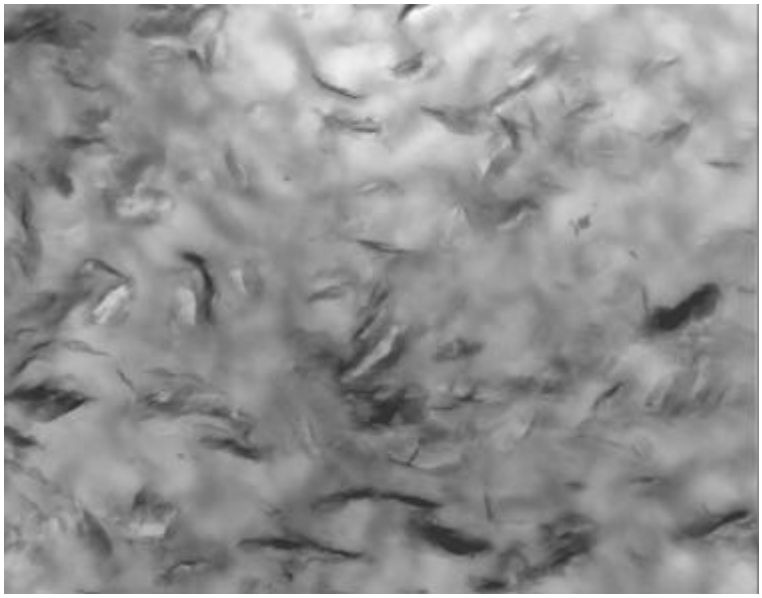

Figure 3. TEM of PA-6/5 % MMT (SCPX 2171) showing the intercalated tactoids dispersed in the PA-6.

3.1.2. Cone Calorimetry

Preparation of intercalated PA-6 nanocomposites allows comparison to the delaminated PA-6 nanocomposite (UBE) which is prepared by the *in situ* method. The comparison of the heat release rate (HRR) behavior of the intercalated and the delaminated PA-6 nanocomposite is shown in Figure 4. The HRR curves are not significantly different. This indicates that intercalated and delaminated nanomorphologies are equally effective at reducing the flammability (HRR) of PA-6 nanocomposites made using MMT. However, a statistically significant difference in ignition times (t_{ign}) is evident between the intercalated and delaminated nanomorphologies from the HRR data in Figure 4. Specifically, the intercalated sample had an t_{ign} of 40 s compared to the t_{ign} of 80 s for the delaminated sample. The t_{ign} of the delaminated sample is similar to that for the pure PA-6 (t_{ign} 70 s). This shorter t_{ign} may be due to some physical effect (thermal conductivity, radiation absorption) or a chemical effect (thermal stability, volatile organic treatment).[8] In terms of possible chemical effects both the different methods of preparing the nanocomposites and the different MMT treatments may contribute to the earlier t_{ign}; the delaminated PA-6 nanocomposite sample is made via the *in situ* polymerization method, which uses an amino acid MMT treatment that becomes covalently bonded to the PA-6 as an end-group during the polymerization. The intercalated PA-6 nanocomposite, prepared via melt blending, at 246 °C, with a quaternary alkyl ammonium treated MMT, does not bond the MMT treatment to the polymer. This may reduce t_{ign}, since the decomposition temperature of the quaternary alkyl ammonium treated MMT (250 °C) is 100 °C lower than that for the delaminated PA-6 nanocomposite.[1] An additional effect may be due to processing. The melt blending process temperature (246 °C), used to make the intercalated PA-6 nanocomposite, is very close to the decomposition temperature of the quaternary alkyl ammonium treated MMT; decomposition products generated during processing may supply volatile fuel early in the Cone experiment and shorten t_{ign}.

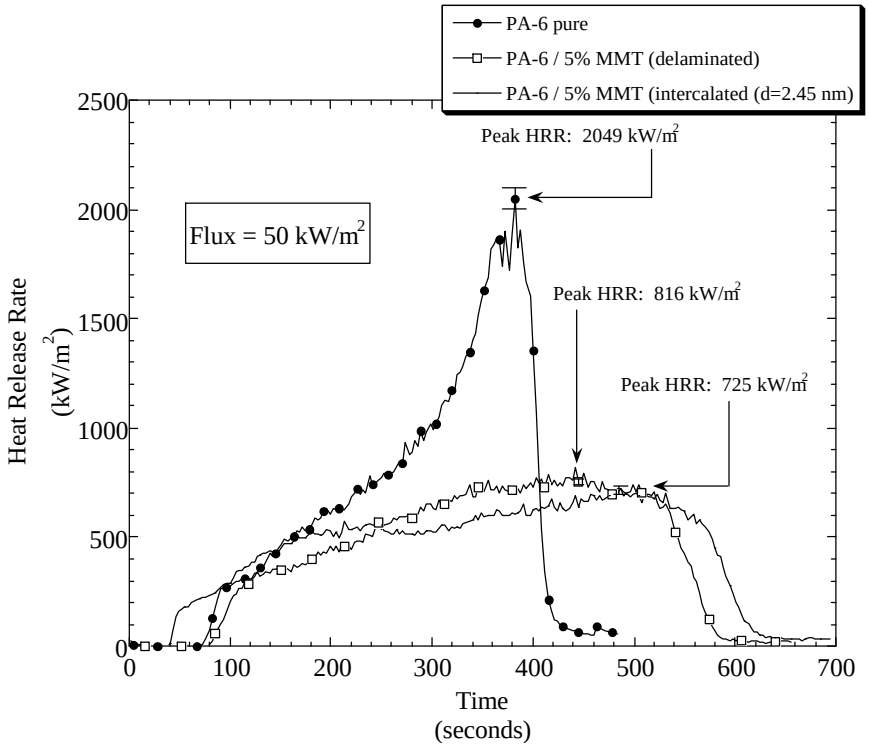

Figure 4. Heat release rate (HRR) data for pure PA-6, and intercalated and delaminated PA-6/MMT (mass fraction 5%) nanocomposites.

The effect of varying the MMT loading in PA-6 nanocomposites on the HRR is shown in Figure 5. The reduction in peak HRR improves as the mass fraction of MMT increases. The additional improvement for the PA-6/MMT nanocomposite with a MMT mass fraction 10 % is somewhat unusual when compared to the result for the other polymer nanocomposites we evaluated (see below). Usually there is little improvement above the 5 % loading level.

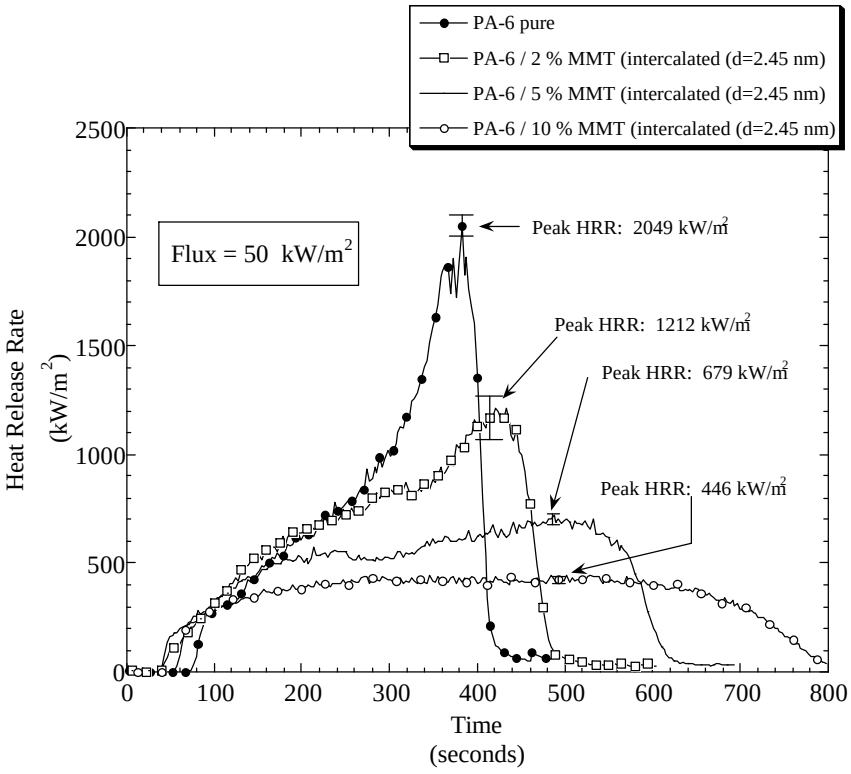

Figure 5. Heat release rate (HRR) data for pure PA-6, and intercalated PA-6/MMT nanocomposites (mass fractions 2 %, 5 %, and 10 %).

In our initial studies on the flammability of PA-6 nanocomposites (UBE) we found that a layered-silicate carbonaceous residue formed during combustion.[9] However, there was very little additional carbonaceous char formed. We felt the use of an additive that would introduce additional carbonaceous char might enhance the effectiveness of the nanocomposite. To this end, PA-6 and polyphenylene oxide (PPO) were extruded with the organic modified MMT. The HRR properties of these PA-6/PPO/MMT nanocomposites are shown in Figure 6.

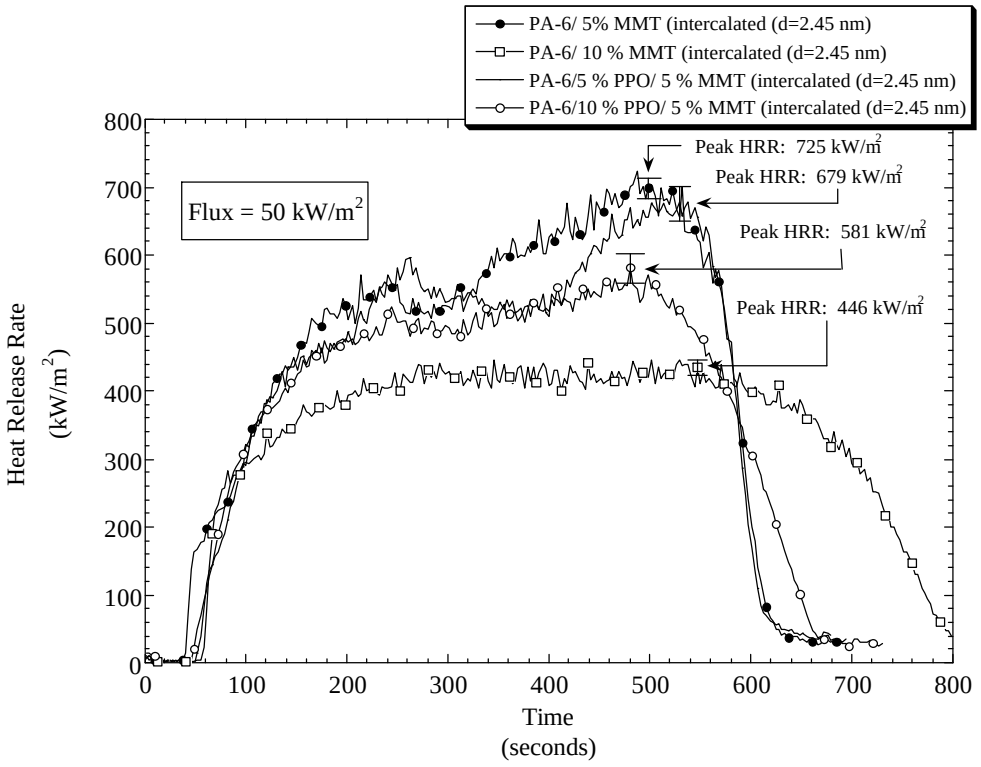

Figure 6. The HRR plots for PA-6/5 % MMT, PA-6/10 % MMT, PA-6/5 % PPO/5 % MMT and PA-6/10 % PPO/5 % MMT nanocomposites. All samples have intercalated nanomorphologies.

The introduction of PPO into the PA-6/MMT nanocomposites gives no improvement in HRR when added at the 5 % level. When 10 % PPO is added the HRR is lowered significantly. However this is in part due to the inherent lower HRR of PPO versus PA-6. The data in Figure 6 show that the PA-6/10 % MMT actually out performs even the PA-6/10 % PPO/5 % MMT. The char yield of PPO is 40 %; possibly, use of another polymer that has a higher char yield is necessary to see the effect we envisioned.

In addition to measuring HRR the Cone Calorimeter also measures other fire-relevant properties such as mass loss rate (MLR), specific heat of combustion (H_c), and specific extinction area (SEA, a measure of smoke density), carbon monoxide yield, and carbon dioxide yield. The HRR and the MLR data for the PA-6 nanocomposites discussed are the only parameters affected by the presence of nano-dispersed MMT in PA-6. The MLR data follows the loss of fuel from the condensed phase into the gas phase. In this case the MLR follows the volatilization of PA-6 decomposition products (primarily caprolactam). Figure 7 shows the MLR data for the intercalated and delaminated PA-6/MMT (mass fraction 5 %) nanocomposites.

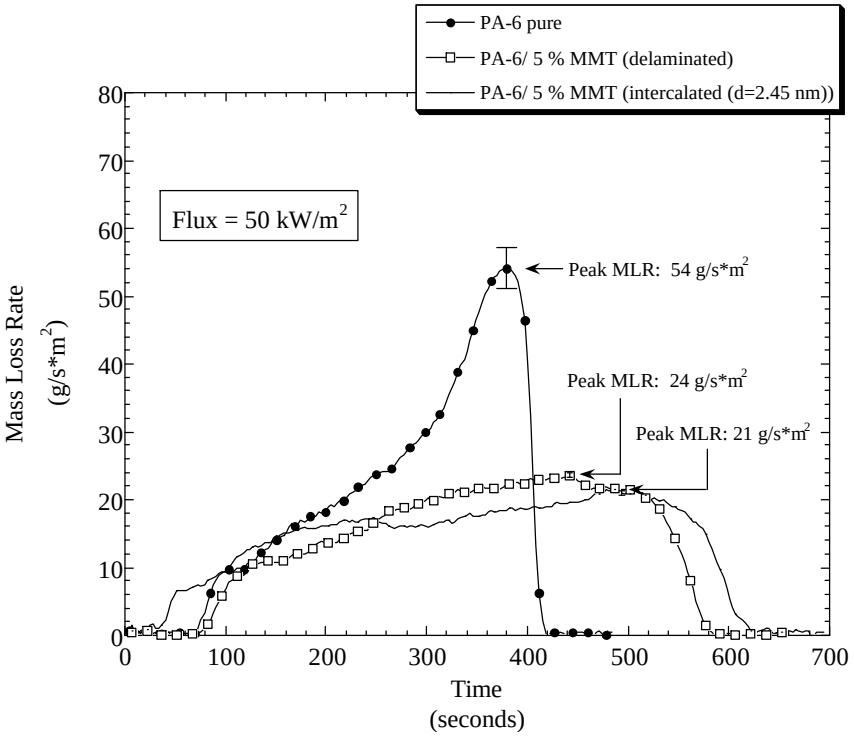

Figure 7. MLR data for PA-6 pure, intercalated and delaminated PA-6/MMT (mass fraction 5%) nanocomposites.

Comparison of Figure 4 to Figure 7, and recalling that none of the other parameters measured in the Cone were affected by the presence of nano-dispersed MMT, reveals that the nano-dispersed MMT reduces the HRR by reducing the MLR (fuel feed rate) of the nanocomposite. This is consistent with the results we found in our initial studies of the delaminated PA-6/MMT.[9]

3.1.3. Gasification

For Gasification analysis, we typically measure MLR, and a video is taken of the sample inside the apparatus during the gasification. We evaluated the above series of PA-6/MMT nanocomposites using the Gasification apparatus and found that the MLR data showed the same trends as observed in the Cone experiments. Furthermore, we observed, from the video data, that a black-residue formed on the sample surface at about 150 s into the gasification experiment. The formation of this residue coincided with the reduced MLR. An additional observation we made is that the mass loss initiates earlier for all the PA-6/MMT nanocomposites as compared to the pure PA-6. This is analogous to the observed shorter t_{ign} for all the PA-6/MMT nanocomposites found in the Cone data.

3.1.4. UL94 testing[10]

The data from standard UL94 flammability testing of the PA-6 nanocomposites are shown in Table 11 through Table 14. The UL-94 test is a qualitative pass/fail test, and while it provides quantities (burn times), the data from this test cannot be held up to a strict error analysis. The PA-6/5 % MMT nanocomposite produces a V-2 rating while the other nanocomposites all fail the UL94 test. It is unclear which measured parameter in the Cone Calorimeter experiments controls performance in the UL94 test. We are in the process of attempting to correlate the UL94 test with the data from the Cone Calorimeter.

Table 11. UL-94 burn data for PA-6/5 % MMT nanocomposite.

Trial #	t_1(s)	Comments	t_2(s)	Comments
1	6	FD, SE	10	FD, SE
2	6	FD, SE	9	FD, SE
3	6	FD. SE	20	FD. SE
4	6	FD, SE	15	FD, SE
5	7	FD, SE	20	FD, SE

t_1 = first ignition burning time. t_2 = second ignition burning time.
BTC: burn to clamp. FD: flaming drip. SE: self extinguishing

Table 12. UL-94 burn data for PA-6/10 % MMT nanocomposite.

Trial #	t_1(s)	Comments	t_2(s)	Comments
1	34	BTC	-	-
2	30	BTC	-	-
3	40	BTC	-	-
4	33	BTC	-	-
5	32	BTC	-	-

Table 13. UL-94 burn data for PA-6/5 % PPO/5 % MMT nanocomposite.

Trial #	t_1(s)	Comments	t_2(s)	Comments
1	40	BTC	-	-
2	30	BTC	-	-
3	15	FD, SE	10	BTC
4	42	BTC	-	-
5	13	FD, SE	11	BTC
6	13	FD, SE	10	BTC
7	40	BTC	-	-
8	13	FD, SE	8	BTC

Table 14. UL-94 burn data for PA-6/10 % PPO/5 % MMT nanocomposite.

Trial #	t_1(s)	Comments	t_2(s)	Comments
1	35	BTC	-	-
2	30	BTC	-	-
3	28	BTC	-	-
4	32	BTC	-	-
5	35	BTC	-	-

3.1.5. Mechanical Property Testing.

Measured mechanical property data are presented in Table 5. Mild increases in strength and stiffness due to filler addition were observed along with a drastic decrease in ductility with clay addition (Fig. 8). The addition of PPO did not have a significant affect on the material properties. Addition of clay slightly increased the maximum stress achieved by the material, (Fig. 9) but significantly reduced the ductility of the material (Fig. 10). Also shown is a rule-of-mixtures computation of modulus based on the modulus of the PA-6, the modulus of the clay, and the amount of

clay in the system (Fig. 11). The enhancement in stiffness follows the rule of mixtures, indicating that the intercalated microstructure did not enhance the mechanical response beyond that which would be expected for normal filler addition.

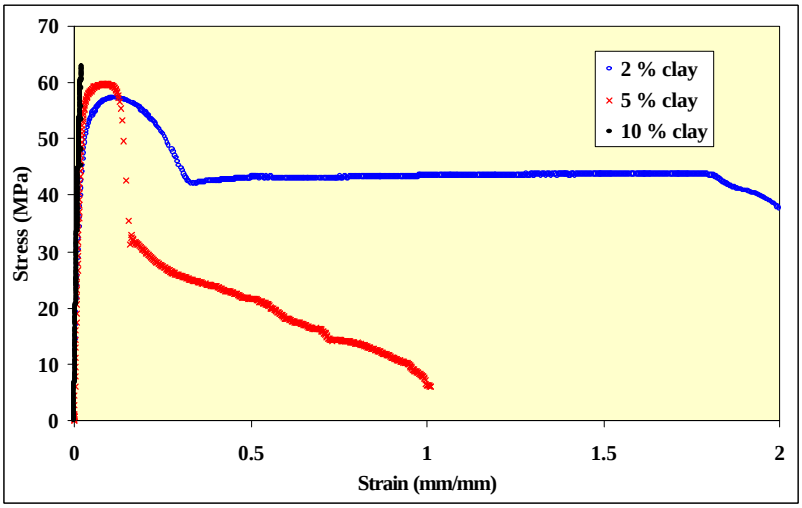

Figure 8. Typical stress-strain response measured for Nylon 6 clay nanocomposites for different clay loadings.

Table 15. Measured values of maximum stress, maximum strain, and elastic modulus for Nylon 6 clay nanocomposites.

	Maximum Stress (MPa)	**Maximum Strain (mm/mm)**	**Elastic Modulus (GPa)**
PA 6 – 2 % clay	58.3 ± 1.1	1.9 ± 1.1	2.4 ± 0.4
PA 6 – 5 % clay	60.8 ± 1.2	0.8 ± 0.5	2.8 ± 0.4
PA 6 – 10 % clay	61.9 ± 3.6	0.4 ± 0.4	4.1 ± 0.6
PA 6/5 % PPO -- 4.75 % clay	58.7 ± 0.9	1.1 ± 0.2	3.0 ± 0.3
PA 6/10 % PPO -- 4.5 % clay	57.9 ± 1.2	0.4 ± 0.2	3.2 ± 0.3

Values are averages and standard deviations for at least 11 samples.

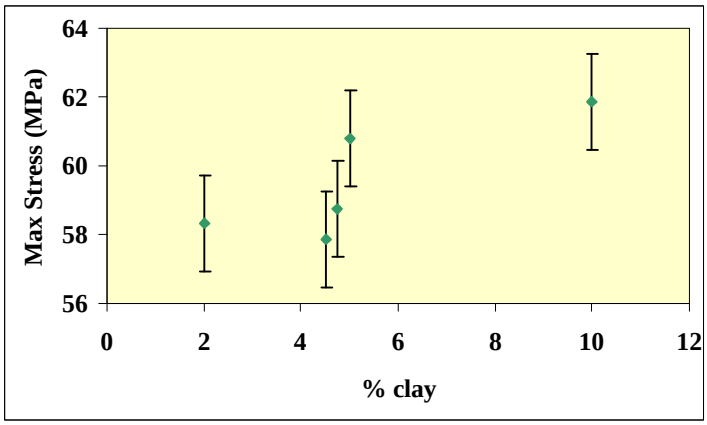

Figure 9. Maximum stress measured for Nylon 6 clay nanocomposites as a function of clay loading.

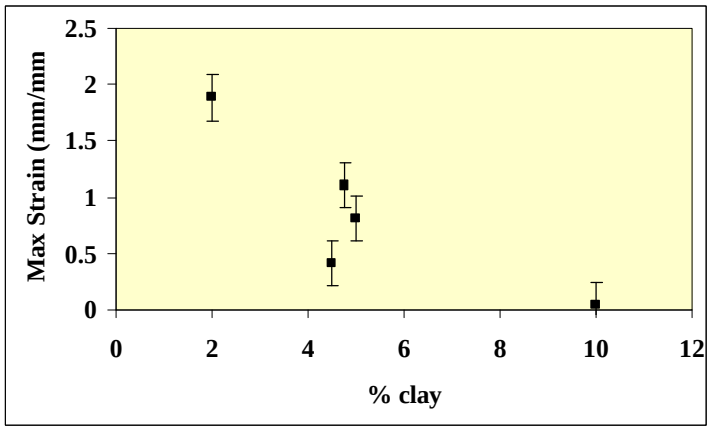

Figure 10. Maximum strain measured for Nylon 6 clay nanocomposites as a function of clay loading.

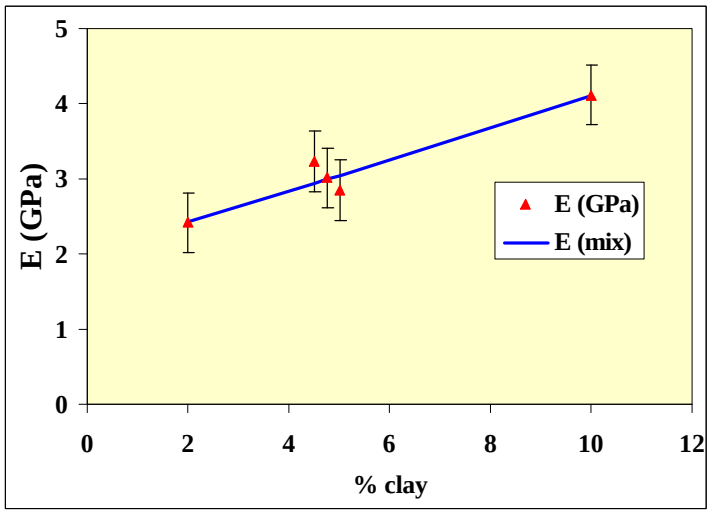

Figure 11. Elastic modulus, E, measured for Nylon 6 clay nanocomposites as a function of clay loading.

3.2. PS nanocomposites

The initial plans (also shown above in section 1.2) for PS nanocomposites at the beginning of Year One included studying the effect of varying the following nanocomposite parameters (critical experiment number in parenthesis): (5) nanocomposites with different melt viscosities, and (6) nanocomposites with different silicate loading levels. Both of these sets of experiments have been completed in year one.

3.2.1. Characterization

The PS nanocomposite samples, of differing molecular weight, each containing 5 % of an organically treated montmorillonite clay, were analyzed by XRD from 1° to 30° (2 theta). XRD indicated the samples contained intercalated PS nanocomposite (Fig. 12). The d-spacings increased from 2.42 nm (d-spacing for organically treated clay: SCPX2197) to 3.27 nm and 3.34 nm for the high molecular weight and low molecular weight polystyrene samples, respectively.

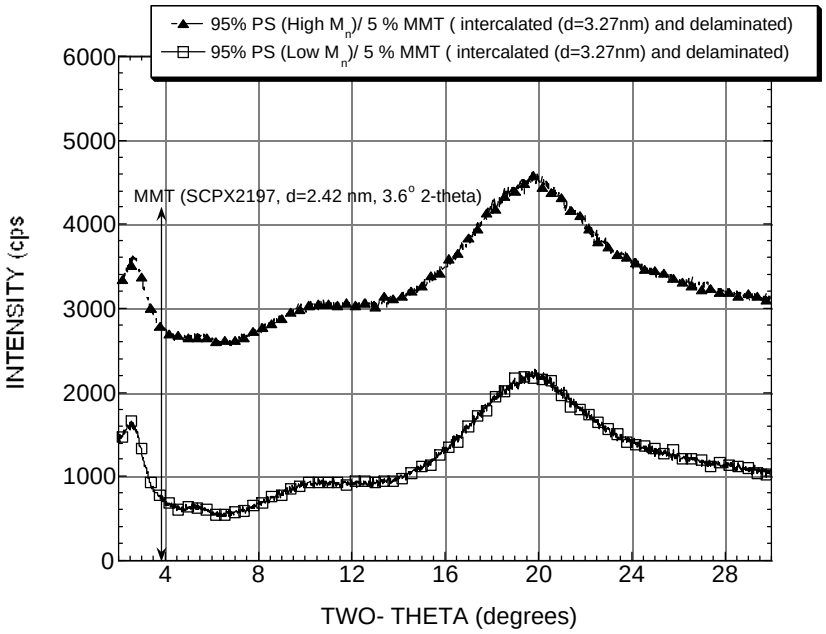

Figure 12. X-ray diffraction data for PS/5 % MMT nanocomposites (high Mw, and low Mw).

TEM indicates that the PS/5 % MMT nanocomposites have a mixed nanomorphology. At low magnification, TEM shows that the clay is well dispersed throughout the polymer (Fig. 13A). Individual clay layers along with two and three layer particles are observed well dispersed (delaminated) in the polymer matrix (Fig. 13B). In addition, large intercalated tactoids (multi-layer particles) as seen in Figure 13A are also visible (Fig. 14). This mixed nanomorphology reflects results seen with PS/MMT nanocomposite samples prepared previously.[11]

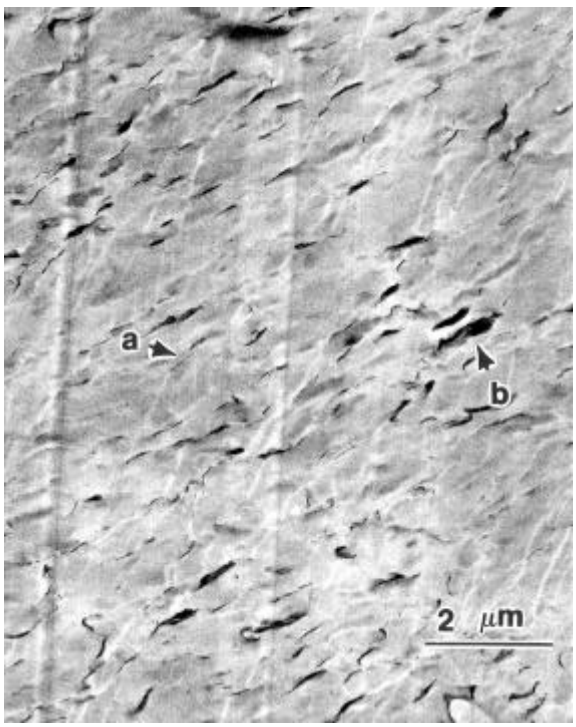

A.

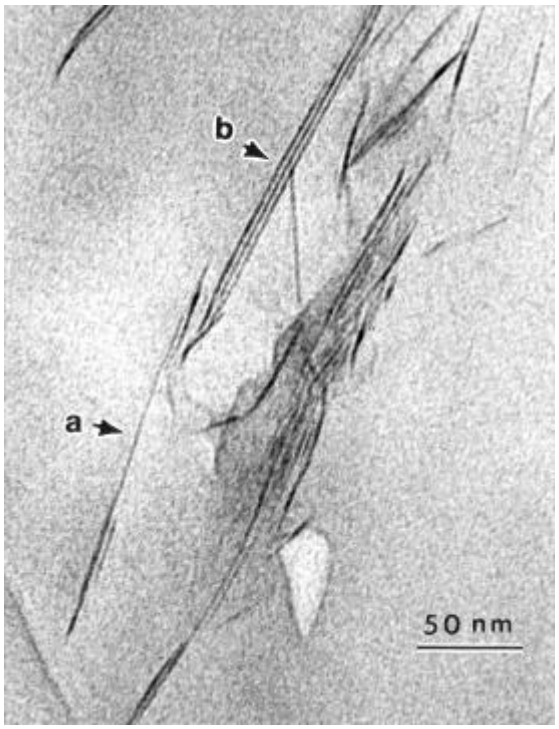

B.

Figure 13. **A**. Low magnification TEM image of PS + 5 % Clay. Note small multi-layer tactoids (a) as well as larger tactoids (b). **B**. High magnification TEM image of PS + 5 % Clay. Single layers (a) as well as small layer stacks (b) can be observed.

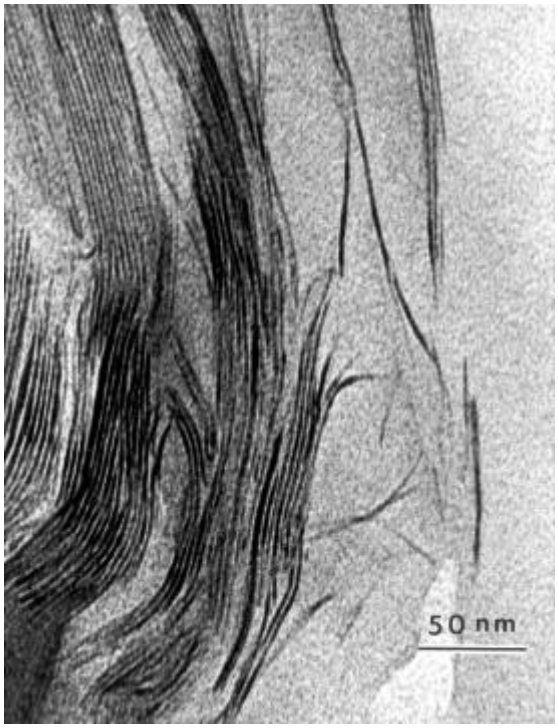

Figure 14. High magnification TEM image of PS + 5 % Clay.

Thermogravimetric analysis (TGA)[12] of the PS nanocomposites is shown in Table 16. These data reveal a 19 °C increase in thermal stability for both molecular weight PS/MMT samples. This is less than half of the 49 °C increase in thermal stability observed previously for PS/ MMT nanocomposites.[11]

Table 16. TGA data of PS/ 5 % MMT nanocomposites.

Sample	TGA derivative maxima
1×10^5 Mw PS	412 °C
1×10^5 Mw PS/5 % MMT nanocomposite	431 °C
1.7×10^5 Mw PS	414 °C
1.7×10^5 Mw PS/5 % MMT nanocomposite	433 °C

This may be due to the different processing methods used in each study. The PS/5 % MMT nanocomposites made in this project were compounded at 205 °C in a 25 mm twin screw extruder; whereas the earlier PS/ MMT nanocomposites were compounded at 150 °C to 170 °C in a mini-extruder under nitrogen. Indeed, gel permeation chromatography (GPC)[13] analysis of the samples (see Figure 15 and Figure 16) extruded at higher temperature, without a nitrogen flow in the extruder, showed some evidence of degradation in the form of lower Mw. This is consistent with another study which found that low temperature processing was necessary to prevent PS degradation when organo-MMT was present.[14]

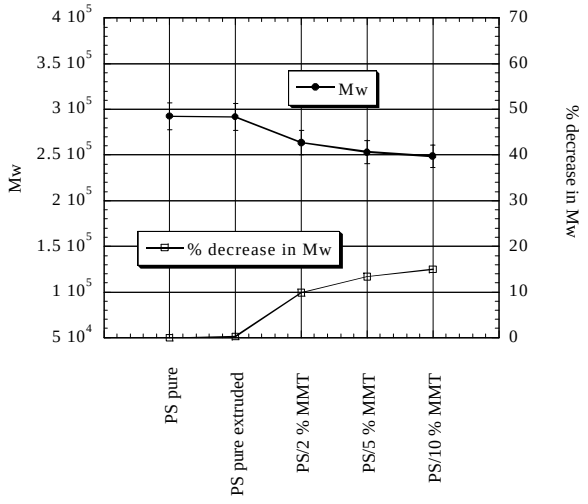

Figure 15. GPC data for high Mw PS and PS/5 % MMT nanocomposites.

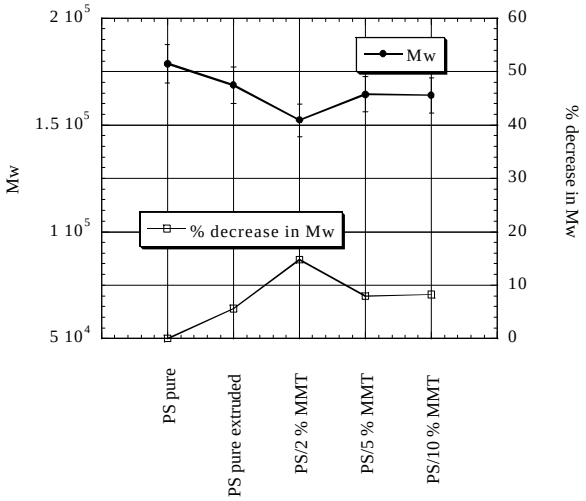

Figure 16. GPC data for low Mw PS and PS/5 % MMT nanocomposite

3.2.2. Cone Calorimetry

The preparation of PS/ MMT nanocomposites with different Mw, and with different MMT loading levels allows study of the effect of melt viscosity[15] combined with the effect of loading. The HRR data for pure PS and PS/ 10 % MMT nanocomposites for both molecular weights is shown in Figure 17. The factor of 3 to 4 reduction in the peak HRR for the PS/ 10 % MMT nanocomposites compared to

the pure PS is impressive. Furthermore, even though there is little difference in the HRR of the two different molecular weights of pure PS, there is a significant difference in the flammability of the two different molecular weights of the PS/ 10 % MMT nanocomposites. The high Mw nanocomposite has about a 30 % lower HRR throughout the first 400 s of the combustion experiment compared to the low Mw sample. This may indicate that the viscosity of the molten degrading material in the burning nanocomposite is significantly different for the two samples, and that this has a significant effect on the rate that volatile decomposition products can escape into the gas phase. This longer residence time for decomposition products may provide the opportunity for other secondary reactions to occur, such as those which form char (see gasification section).

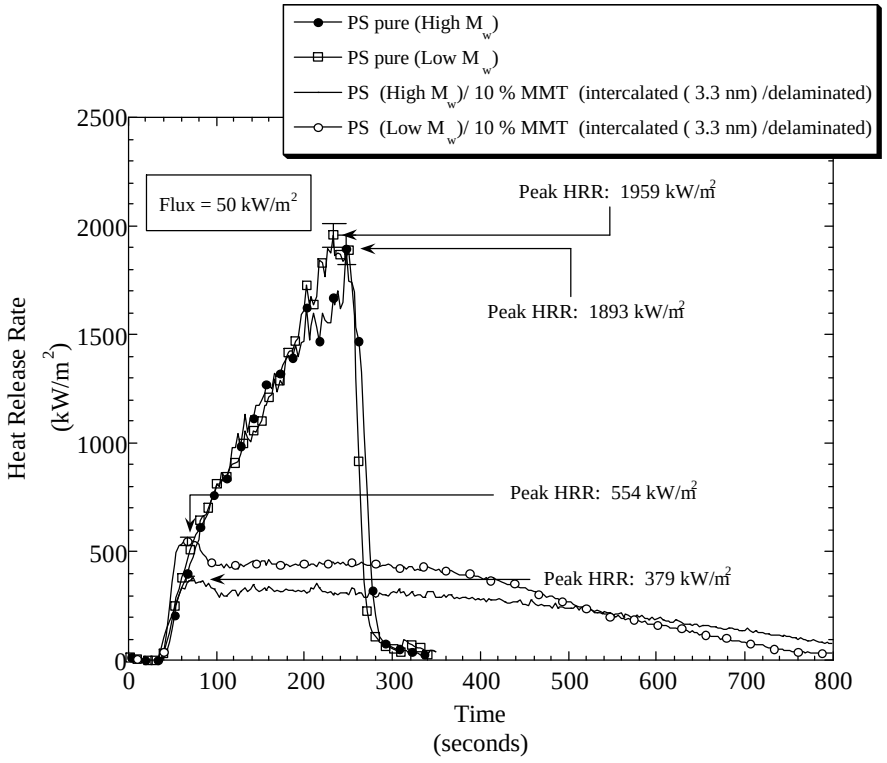

Figure 17. HRR plots for pure PS and PS/ 10 % MMT nanocomposites (low Mw and high Mw).

The HRR data for the high Mw PS/ MMT nanocomposites with 2 %, 5 %, and 10 % clay loading are shown in Figure 18. The reduction in peak HRR improves as the mass fraction of MMT increases. The additional improvement for the PS/MMT nanocomposite with 10 % MMT only occurs during the first 100 s of the burn. This is typical of the result for the other polymer nanocomposites we evaluated (see below), except for PA-6/MMT nanocomposites. A leveling off of improvement in properties at 5 % is a common result for layered-silicate nanocomposites, regardless of the property. As impressive as the HRR data are for the PS system, the gasification data taken on these samples are the most telling regarding the novelty of this approach to flame retarding PS.

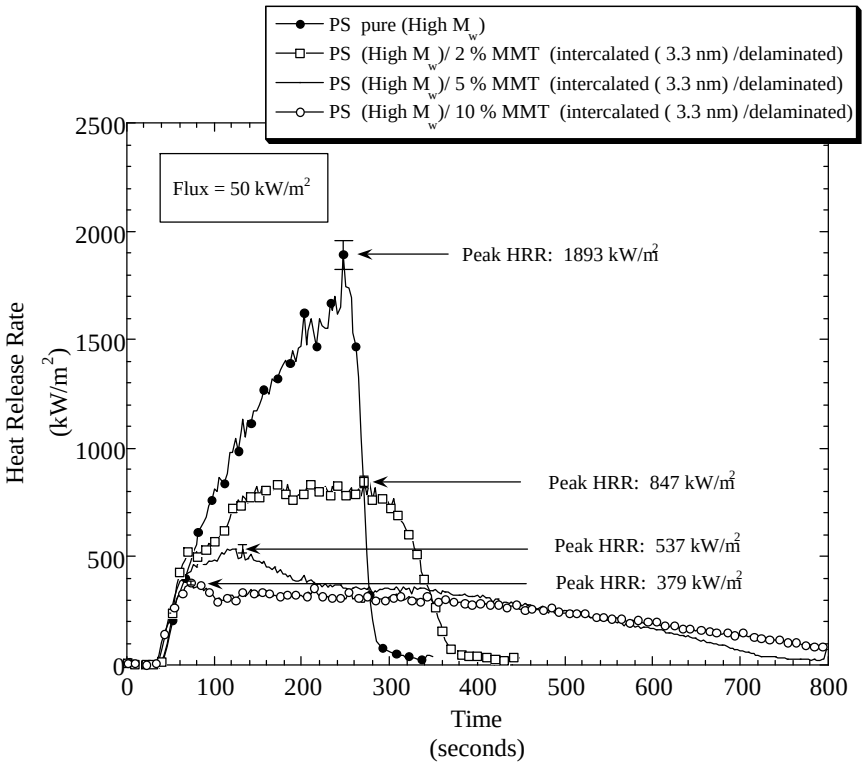

Figure 18. HRR plots for the high Mw pure PS, and the high Mw PS/ MMT nanocomposites with 2 %, 5 %, and 10 % clay loading.

3.2.3. Gasification

The MLR data from the gasification of PS/MMT nanocomposites show the identical trends to those found in the HRR data from the Cone (see Figure 17 and Figure 18). However, the digitized video images taken during the gasification of the low Mw PS/5 % MMT nanocomposite show the most important effect of the nano-dispersed clay on the PS degradation; in contrast to the rapid-boiling liquid layer observed for the pure PS, the PS/5 % MMT sample appears to solidify and converts to a black solid residue very early in the experiment, at 90 s (Figure 19). Once this residue (char) forms, the MLR slows to 25 % of that for pure PS, and as stated before it is this reduced MLR, or fuel feed rate, that is responsible for the dramatic reduction in the HRR. The video images and the gasification residue yields for the PS/MMT nanocomposites (Figure 19) show that the otherwise non-char forming PS is converted to a charring system by the nano-dispersed clay. A slight improvement (1 % to 2 %) in the char yield for the PA-6/MMT nanocomposites was observed in our initial experiments and in those reported here (above). But, very few other flame retardant additives are capable of causing PS alone (without a carbonific) to give carbonaceous char, especially at this low a loading and with such dramatic reduction in flammability.

A Mw effect was also observed in the gasification experiments for the PS nanocomposites. The high Mw PS nanocomposite swelled, or intumesced, to a greater extent than the low Mw PS nanocomposite during the gasification and charring process. This may indicate a higher melt viscosity for the sample that swelled more, and suggests one reason that the decomposition products escaped the condensed phase at a slower rate (i.e., the MLR was lower).

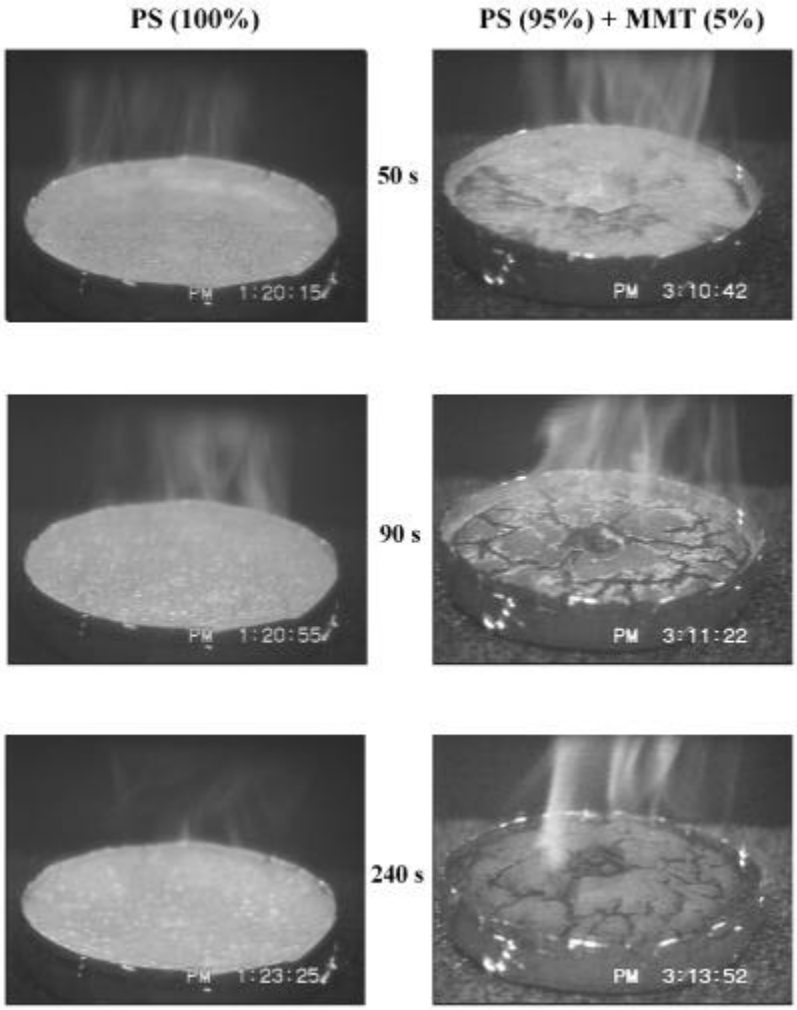

Figure 19. Digitized images from nitrogen gasification at a flux of 50 kW/m^2 of pure PS (low Mw) and PS/5 % MMT nanocomposite (low Mw).

3.2.4. UL94 testing[10]

The data from standard UL94 flammability testing of the PS/MMT nanocomposites are shown in Table 17 and Table 18. The PS/MMT nanocomposites all fail the UL94 test. As stated above it is unclear what measured parameter(s) in the Cone data controls performance in the UL94 test. We are in the process of attempting to correlate the UL94 test with the data from the Cone Calorimeter. It is possible a threshold needs to be reached in terms of a maximum HRR in order to obtain a V-0 rating.

Table 17. UL-94 burn data for PS/2 % MMT (low Mw)

Trial #	t_1(s) avg.	Comments	t_2(s)	Comments
1, 2	16	FD, SE	11	BTC
3-5	28	BTC	-	-

t_1 = first ignition burning time. t_2 = second ignition burning time.
BTC: burn to clamp. FD: flaming drip. SE: self extinguishing, burn times are ± 10 %.

Table 18. UL-94 burn data for PS/ MMT nanocomposites.

Sample	Avg. t_1(s)	Comments	t_2(s)	Comments
PS/5 % MMT (low Mw)	29	BTC	-	-
PS/10 % MMT (low Mw)	33	BTC	-	-
PS/2 % MMT (high Mw)	30	BTC	-	-
PS/5 % MMT (high Mw)	35	BTC	-	-
PS/10 % MMT (high Mw)	36	BTC	-	-

3.3. PP nanocomposites

The focus of the experiments for the PP nanocomposites was to study the effect of varying the following nanocomposite parameters (critical experiment number in parenthesis): (1) intercalated versus delaminated nanocomposites, and (6) nanocomposites with different silicate loading levels.

3.3.1. Characterization

Each PP/MMT nanocomposite prepared was completely characterized by XRD and TEM. The XRD data, and a summary of the nanomorphology, based on TEM and XRD, of each sample are shown in Table 19. TEM shows that the PP/5 % MMT samples, made using either organo-treated MMT, were intercalated nanocomposites with little or no delaminated layers (Figure 20). TEM of the PP compatibilized using PP-g-MA (PP/15 % PP-g-MA/MMT) revealed that they all had a mixed intercalated/delaminated nanomorphology, due to the presence of the PP-g-MA (Figure 21). The d-spacings for the intercalated tactoids in these samples are also shown in Table 19. In addition, GPC was done before and after extrusion to look for degradation. Although, the PP/15 % PP-g-MA/MMT samples were darker than expected little change in Mw was found.

Figure 20. TEM of PP/5 % MMT (SCPX 1980) showing intercalated tactoid structure.

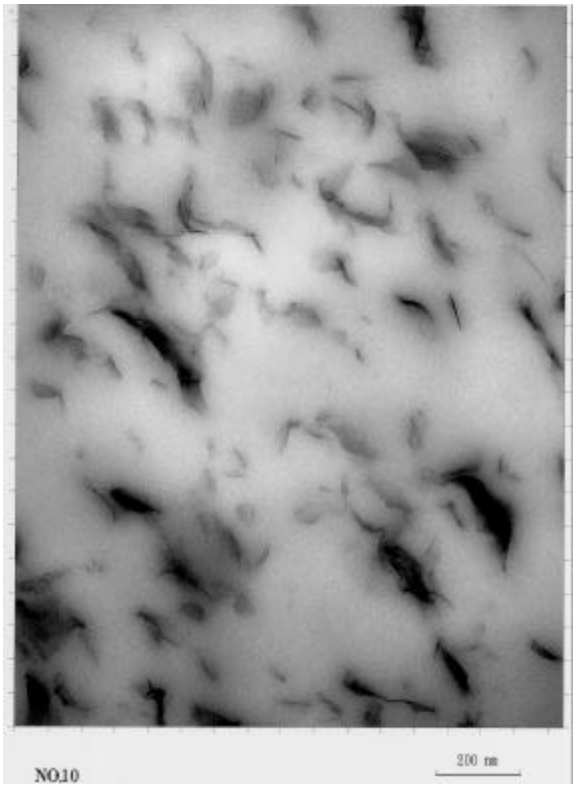

Figure 21. TEM of PP/15 %PP-g-MA/5 % MMT (ODA Nanomer) showing delaminated /intercalated nanomorphology.

Table 19. XRD and nanomorphology based on TEM of PP/MMT nanocomposites.

Sample	**Organo-clay (d-spacing, nm)**	**PP/MMT d-spacing (nm)**	**Change in d-spacing (nm)**	**TEM**
PP/5 % MMT (SCPX1980)	Quaternary alkyl ammonium MMT (2.54)	2.63	0.09	Intercalated
PP/15 % PP-g-MA/5 % MMT (SCPX1980)	"	3.68	1.14	Intercalated/ delaminated
PP/15 % PP-g-MA/2 % MMT (SCPX1980)	"	-	-	Intercalated/ delaminated
PP/15 % PP-g-MA/10 % MMT (SCPX1980)	"	3.22	0.68	Intercalated/ delaminated
PP/5 % MMT (ODA Nanomer)	ODA MMT (1.85)	2.71	0.86	Intercalated
PP/15 % PP-g-MA/5 % MMT (ODA Nanomer)	"	3.56	1.71	Intercalated/ delaminated
PP/15 % PP-g-MA/2 % MMT (ODA Nanomer)	"	3.56	1.71	Intercalated/ delaminated
PP/15 % PP-g-MA/10 % MMT (ODA Nanomer)	"	3.50	1.65	Intercalated/ delaminated

3.3.2. Cone Calorimetry

The comparison of intercalated versus delaminated nano-morphologies, for PP nanocomposites, is not as clean as it is for the PA-6 nanocomposites (Figure 4), since no purely delaminated sample was prepared. Yet the HRR data shown in Figure 22 reveal that the mixed - intercalated and delaminated - sample (PP/15 % PP-g-MA/5 % MMT-ODA Nanomer) has a significantly lower HRR than the intercalated sample (PP/5 % MMT-ODA Nanomer) from 200 s to 400 s. This was also true for the PP nanocomposites made using SCPX1980. This is in contrast to the HRR results for intercalated versus delaminated PA-6 nanocomposites, where little difference was found between the nano-morphologies (Figure 4).

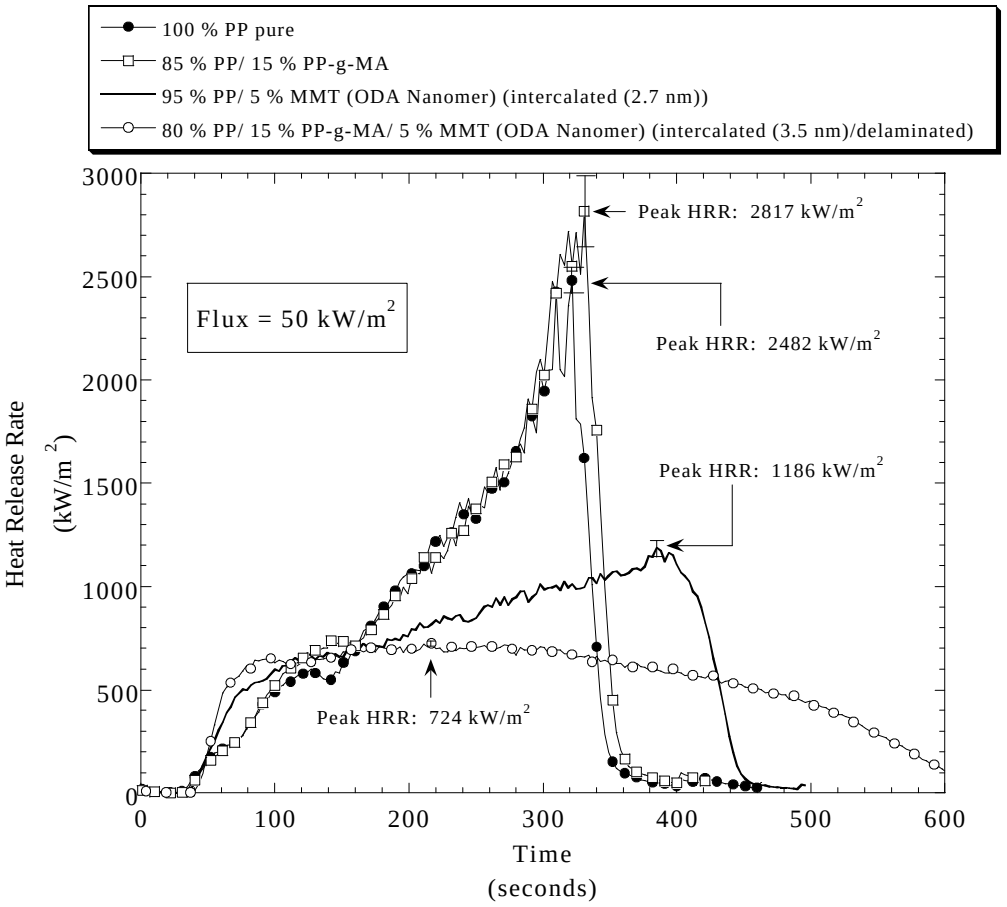

Figure 22. HRR plots for pure PP, PP/15 % PP-g-MA, PP/ 5 % MMT (intercalated) nanocomposite and PP/PP-g-MA/ 5% MMT (intercalated /delaminated) nanocomposite.

The HRR data for the PP nanocomposites with different MMT loading levels are shown in Figure 23. While the reduction in HRR is greater for the 5 % MMT sample compared to the 2 % MMT sample, only a small benefit is derived from increasing the loading from 5% to 10 %. We see this in all of the nanocomposite systems we studied in this program except for the PA-6 nanocomposites (Figure 5).

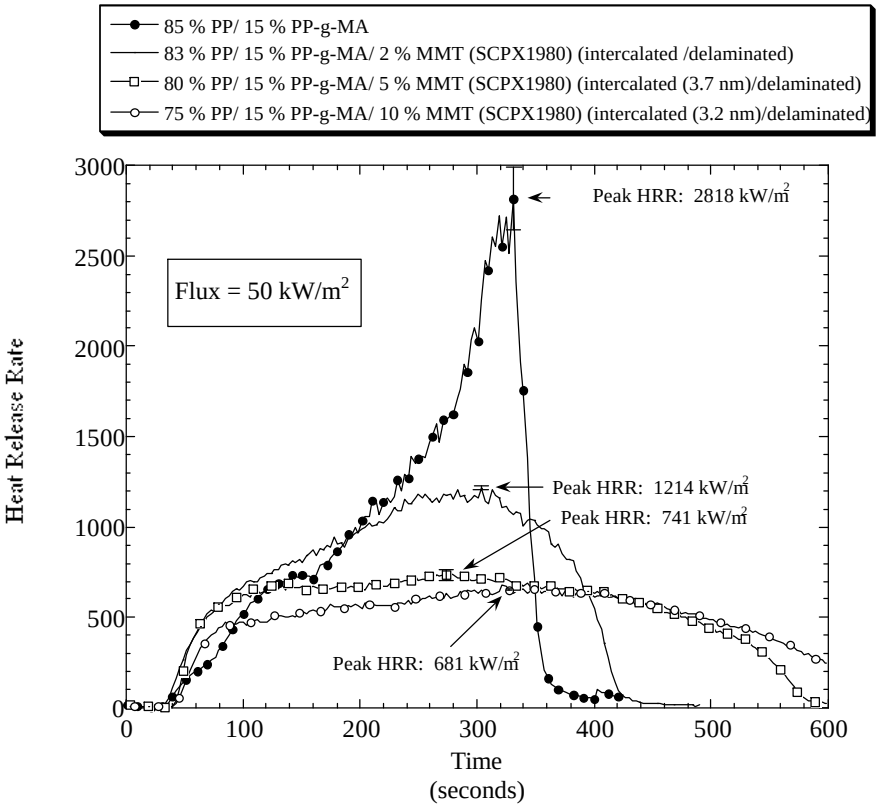

Figure 23. HRR plots for PP/15 % PPgMA, and PP/PPgMA/ 5% MMT (intercalated /delaminated) nanocomposite with 2 % 5 %, and 10 % MMT.

An additional observation discernable from the HRR data in Figure 23 is that for the first 60 s of the burn the HRR for the nanocomposites is higher than that for the PP/PPgMA sample. This may be due to some physical effect (thermal conductivity, radiation absorption) or a chemical effect (thermal stability, volatile organic treatment). This is similar to the shorter ignition times (t_{ign}) we see in the PA-6 nanocomposites (Figure 5). The use of additional char enhancing additives, or conventional flame retardants which delay ignition could counteract these effects. Indeed, recently published reports show that the use of intumescents, melamine, poly(tetrafluoroethylene) (PTFE), or red phosphorus combined with nanocomposites gives UL 94 V-0 ratings in a variety of polymer systems.[16,17,18,19]

3.3.3. Gasification

The reduced MLRs for PP/MMT nanocomposites found in the gasification experiments closely follow the reductions in HRR from the Cone Calorimeter experiments discussed above. The formation of additional carbonaceous char was also seen in the PP nanocomposites. This is best observed in the digitized images from the videos of the gasification experiments (Figure 24), which show similar results to those for PS/MMT nanocomposites (Figure 19). The critical role MMT and PPgMA play in forming carbonaceous char is evident by comparing the left image to the center image. Comparing the center and right images shows the effect of MMT loading on the volume and quality of the char formed. However, while both PPgMA and MMT must be present for additional carbonaceous char to

be formed for the PP/MMT nanocomposites, no compatibilizer is required, either for carbonaceous char formation, or for intercalation/delamination for the PS-nanocomposites.

The higher HRR behavior early in the burn, noted above, is also observed as higher MLR in the first part of the gasification experiments for the PP/MMT nanocomposite samples. Again, this may be from the physical or chemical effects discussed above.

Figure 24. Digitized photos of gasification residues from PP/5 % MMT (SCPX1980) (left), PP/15 % PPgMA/2 % MMT (SCPX1980) (center), and PP/15 % PPgMA/5 % MMT (SCPX1980) (right).

3.3.4. UL94 testing[10]

The UL 94 testing of the PP/MMT nanocomposites is shown in Table 20. Slower burning times are observed for some of the samples, but no self extinguishing behavior is found. Again, the use of additional char enhancing additives, or conventional flame retardants should improve performance in the UL 94 test. We are in the process of looking for some correspondence between UL 94 behavior and data from the Cone experiments.

Table 20. UL-94 burn data for PP/ MMT nanocomposites

Sample	**Avg. t_1(s)**	**Comments**	**t_2(s)**
PP/5 % MMT(SCPX1980)	48	BTC	-
PP/15 % PPgMA/5 % MMT(SCPX1980)	47	BTC	-
PP/15 % PPgMA/10 % MMT (SCPX1980)	64	BTC	-
PP/5 % MMT(ODA Nanomer)	59	BTC	-
PP/15 % PPgMA/5 % MMT(ODA Nanomer)	56	BTC	-
PP/15 % PPgMA/10 % MMT(ODA Nanomer)	55	BTC	-

t_1 = first ignition burning time. t_2 = second ignition burning time. Burn times are an average of 5 runs.
BTC: burn to clamp. FD: flaming drip. SE: self extinguishing, reproducibility of burn times is ± 10 %.

3.4. EVA nanocomposites

The plan for PE/MMT nanocomposites for year one was to study the effect of crosslinking on the flammability (critical experiment 4). Variation in crosslink density was introduced by exposing the samples to electron beam irradiation (beam dosage: 25 kGy [2.5 MRad], 39 kGy [3.9 MRad], and

64 kGy [6.4 MRad]). A copolymer, ethylene vinyl acetate (EVA, 18 % VA) was used instead of pure PE to improve the compatibility of the polymer with the MMT. The effect of varying the MMT loading was also examined. In addition, the EVA was compounded with several organic-treated MMTs: one from Southern Clay Products, SCPX 2156, a quaternary alkyl ammonium-treated MMT, and two from Nanocor, 1.30E, an octadecyl ammonium-treated MMT, and 1.30D, a dodecyl pyrrolidone-treated MMT. This allowed comparison of clay treatments in terms of their effectiveness in delaminating the clays.

3.4.1. Characterization

Both XRD and TEM were used to characterize the nanomorphology of the EVA/MMT nanocomposites. TEM indicates that the EVA sample containing the ODA treated MMT had good dispersion of the MMT throughout the sample, but with some intact intercalated-tactoids remaining. XRD showed the d-spacing of these intercalated-tactoids to be 3.4 nm.

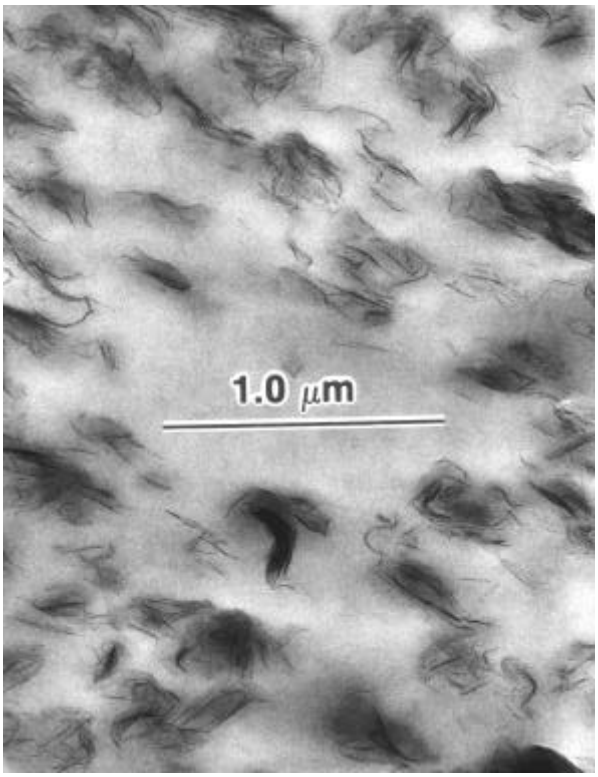

Figure 25. TEM of EVA/5 % MMT (ODA-MMT) showing typical intercalated /delaminated nanomorphology.

The EVA sample containing DDP-treated MMT was not a uniform sample. It appears by TEM (Fig. 25) that the MMT is immiscible in the polymer. Individual clay layers, even in large clay particles, were very hard to see even at high magnification. Further, this sample was not very stable in the presence of the electron beam, and decomposition of the sample occurred during observation with TEM. The XRD of these samples showed a smaller d-spacing (1.24 nm) after extrusion than before, i.e., they appeared to de-intercalate (see Table 21). The volatilization of DDP (b.p. of DDP is 200 °C) during extrusion (melt temperatures: 215 °C to 235 °C) would explain this result.

Table 21. Nanomorphology of EVA/MMT nanocomposites from XRD and TEM.

Sample	Actual Clay Loading [%]	Initial Clay d-spacing [nm]	Final Composite d-spacing [nm]	Nanomorphology
EVA/2 % MMT (SCPX 2156)	2.1	2.24	3.64	Intercalated/ delaminated
EVA/5 % MMT (SCPX 2156)	6.7	2.24	3.43	Intercalated/ delaminated
EVA/10 % MMT (SCPX 2156)	9.7	2.24	3.44	Intercalated/ delaminated
EVA/5 % MMT (I.30 E)	2.2	2.18	3.42	Intercalated/ delaminated
EVA/2 % MMT (I.30 E)	6.4	2.18	3.43	Intercalated/ delaminated
EVA/5 % MMT(I.30 D)	2.1	4.21; 1.46	1.24	-
EVA/2 % MMT(I.30 D)	5.3	4.21; 1.46	1.24	-

3.4.2. Mechanical Properties

Mechanical properties of the EVA/MMT nanocomposites were evaluated by Raychem. The data, (Instron, 5 samples per determination, crosshead speed 25.4 cm/min) are shown in Table 22, Figure 26, Figure 27, Figure 28, and Figure 29. Figures 26 to 29 were provided by Raychem and are in non-SI units.

Table 22. Mechanical Properties data for EVA and EVA/MMT nanocomposites.

Sample	Young's Modulus (**kPa**) [Ksi]	Stress @ Break (**kPa**) [Ksi]	Strain @ Break [%]	Energy @ Break (**N•m**) [lbf-in]
EVA	**15640 ± 4065** [2.27 ± 0.59]	**26871 ± 1378** [3.90 ± 0.20]	785 ± 30	**10.8 ± 1.0** [95.3 ± 9.0]
EVA/2 % MMT (SCPX 2156)	**44165 ± 2205** [6.41 ± 0.32]	**23633 ± 1240** [3.43 ± 0.18]	680 ± 38	**8.7 ± 0.9** [76.8 ± 8.4]
EVA/5 % MMT (SCPX 2156)	**92257 ± 3721** [13.39 ± 0.54]	**21722 ± 896** [3.16 ± 0.13]	641 ± 21	**9.8 ± 0.9** [86.7 ± 8.0]
EVA/10 % MMT (SCPX 2156)	**181414 ± 6980** [26.33 ± 1.00]	**22668 ± 965** [3.29 ± 0.14]	647 ± 16	**10.6 ± 0.4** [93.8 ± 3.4]
EVA/5 % MMT (I.30 E)	**59047 ± 3100** [8.57 ± 0.45]	**20394 ± 1240** [2.96 ± 0.18]	657 ± 31	**7.9 ± 0.8** [69.6 ± 6.8]
EVA/2 % MMT (I.30 E)	**110584 ± 3032** [16.05 ± 0.44]	**17776 ± 551** [2.58 ± 0.08]	627 ± 14	**7.2 ± 0.5** [63.6 ± 4.5]
EVA/5 % MMT(I.30 D)	**38102 ± 4065** [5.53 ± 0.59]	**24046 ± 1171** [3.49 ± 0.17]	715 ± 27	**9.0 ± 0.7** [79.8 ± 6.3]
EVA/2 % MMT(I.30 D)	**40789 ± 2067** [5.92 ± 0.30]	**23357 ± 551** [3.39 ± 0.08]	698 ± 20	**7.9 ± 0.2** [69.9 ± 2.2]

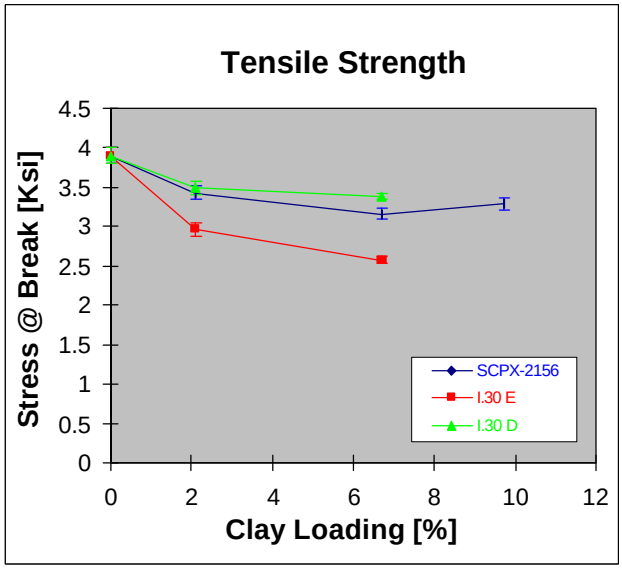

Figure 26. Tensile Strength data for EVA and EVA/MMT nanocomposites.

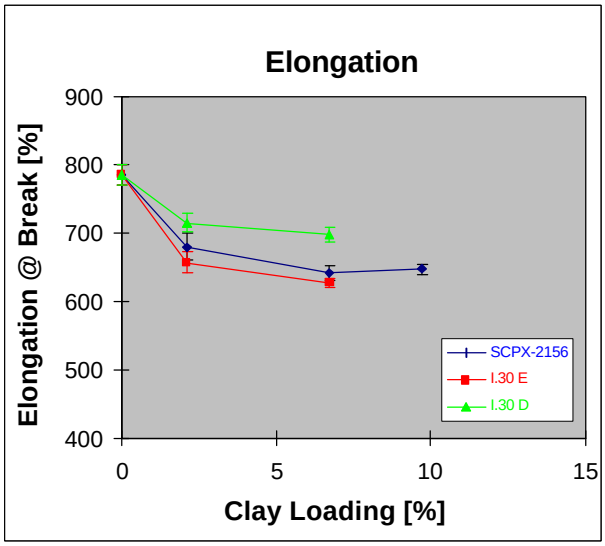

Figure 27. Elongation data for EVA and EVA/MMT nanocomposites.

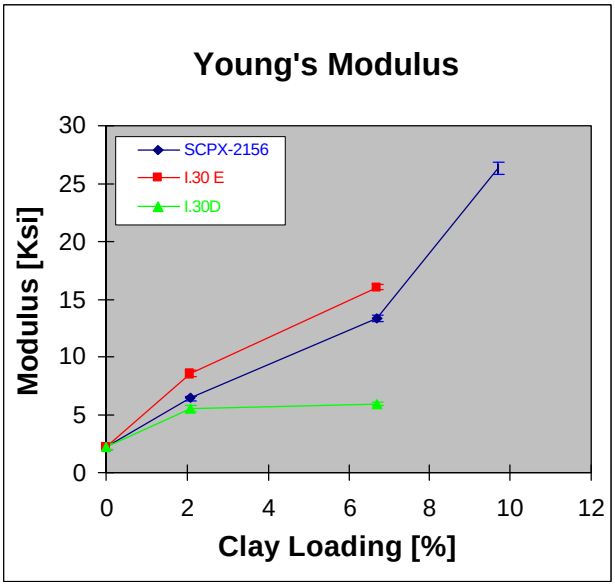

Figure 28. Modulus data for EVA and EVA/MMT nanocomposites.

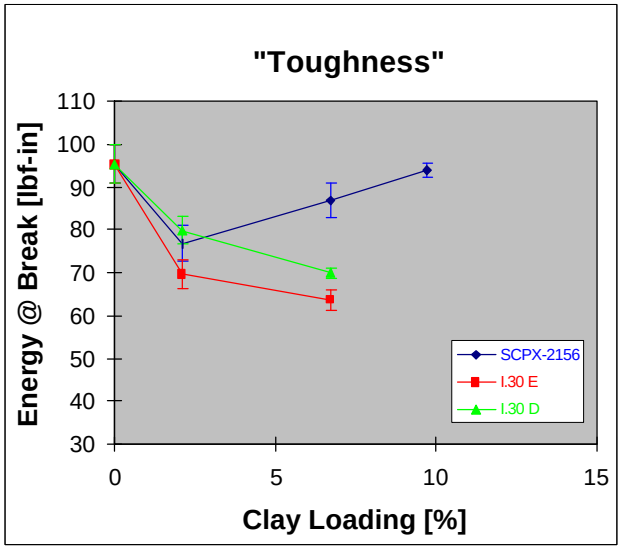

Figure 29. Toughness data for EVA and EVA/MMT nanocomposites.

Mechanical properties of the EVA/MMT nanocomposite samples were also evaluated by NIST using ASTM D 638, testing with type 4 and type 5 samples. The data are shown below in Figure 30 and Table 23.

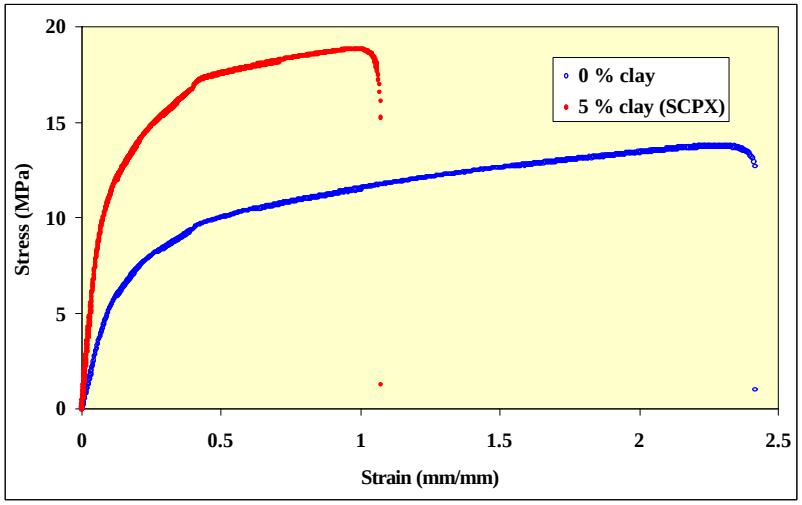

Figure 30. Typical stress-strain response measured for EVA with and without SCPX clay.

Injection molded specimens of EVA (Fig. 28) did not have the ductility that was expected (as shown by the compression molded film samples tested by Raychem shown, Figures 26-29). Addition of clay further reduced ductility. Significant enhancements in strength and stiffness were observed for SCPX clay, but very little enhancement, if any, was observed for DDP and ODA clays. A different injection molding temperature did not significantly impact the performance of the EVA system, nor did drying the resin prior to injection molding. Mechanical property data are shown below in Table 24.

Table 23. Measured values of maximum stress, maximum strain, and elastic modulus for pure EVA and EVA-clay nanocomposites.

	Maximum Stress (MPa)	**Maximum Strain (mm/mm)**	**Elastic Modulus (MPa)**
EVA	13.5 ± 0.6	2.4 ± 0.2	56 ± 3
EVA – 5 % DDP	12.4 ± 0.2	1.8 ± 0.1	67 ± 5
EVA – 5 % ODA	15.2 ± 0.5	1.5 ± 0.1	130 ±.14
EVA – 5 % SCPX	18.5 ± 1.6	1.2 ± 0.1	189 ± 16

Values are averages and standard deviations for at least 6 samples.

3.4.3. Cone Calorimetry

The HRR data for the three non-irradiated EVA/5 % MMT samples are shown in Figure 31. The intercalated/delaminated EVA nanocomposites, EVA/5 % MMT (SCPX 2156) and EVA/5 % MMT (1.30E), behave identically in the Cone; the reduction in HRR for both, compared to the HRR for pure EVA, is 69 %. Interestingly, EVA/5 % MMT (1.30D) does show some reduction in HRR. Previously, in other polymer nanocomposite systems, we have shown that completely immiscible polymer-MMT composites have HRR that are unchanged from the pure polymer. Therefore, the MMT in EVA/5 % MMT (1.30D) may be partially nano-dispersed.

The effect of varying the MMT loading on the HRR of the EVA/MMT nanocomposites (not shown) is the same as that for the PP and PS nanocomposites: the effect improves as the loading is increased from 2 % to 5 %, but no additional effect is seen for the 10 % samples.

As we observed for the PP nanocomposites, the initial HRR for the EVA/MMT samples is higher for the first minute following ignition. This effect is completely counteracted at 120 s into the experiment (80 s after ignition) by the formation of the MMT-reinforced carbonaceous-residue (char). The evidence that this char formation is responsible for the reduced HRR in the case of the intercalated/delaminated EVA nanocomposites, EVA/5 % MMT (SCPX 2156) and EVA/5 % MMT (1.30E), comes from the gasification experiments.

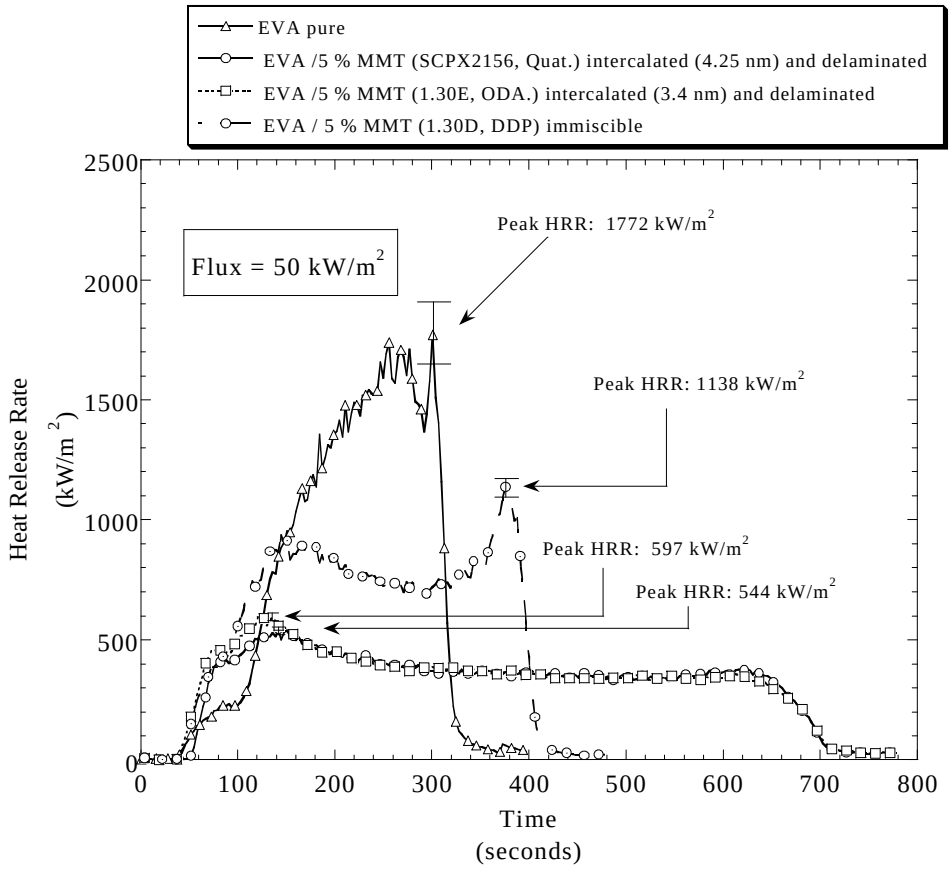

Figure 31. HRR plots for pure EVA, and the three EVA/5 % MMT samples each prepared with a different treated MMT.

3.4.4. Gasification

Visual observation of the gasification experiments performed on the intercalated/delaminated EVA nanocomposites, EVA/5 % MMT (SCPX 2156) and EVA/5 % MMT (1.30E) reveals that char formation begins within 60 s of the initial mass loss. The MLR data for the gasification experiments for the EVA/ MMT samples are shown in Figure 33 and Figure 34. The same relative trends are observed in MLR as we found in HRR (Figure 31) for the three EVA/MMT samples.

A striking difference is evident from examination of the digital photos of the residues from the gasification experiments of EVA/5 % MMT (SCPX 2156) and EVA/5 % MMT (1.30D) shown in Figure 32. A continuous-monolithic carbonaceous-residue forms as a result of gasification of either the EVA/5 % MMT (SCPX 2156) sample (shown below), or the EVA/5 % MMT (1.30E) sample (not shown). However, the poorly dispersed EVA/5 % MMT (1.30D) sample leaves only a light-gray residue which is essentially just MMT. Pure EVA gives a zero residue yield. Clearly, as we observed in the PS/MMT nanocomposites, the otherwise non-char forming EVA is converted to a charring system by the nano-dispersed MMT. Similar residues were formed from the Cone experiments.

The MLR data for the irradiated EVA/MMT samples are shown in Figure 34. Comparison of Figure 33 to Figure 34 reveals that the irradiation increases the peak MLR by 40 % for all the samples. Possibly, some degradation accompanies the radiation-crosslinking which substantially lowers the stability of the irradiated EVA samples. Another method to introduce crosslinking should be considered to revisit this issue. This effect, while unexpected, is similar to flammability results seen with irradiated polyethylene[20] and honeycomb composites.[21] Specifically, these materials showed no great improvement in flammability, but did show a delayed ignition time. The delayed ignition time could be related to the delayed MLR onset seen with these irradiated EVA samples.

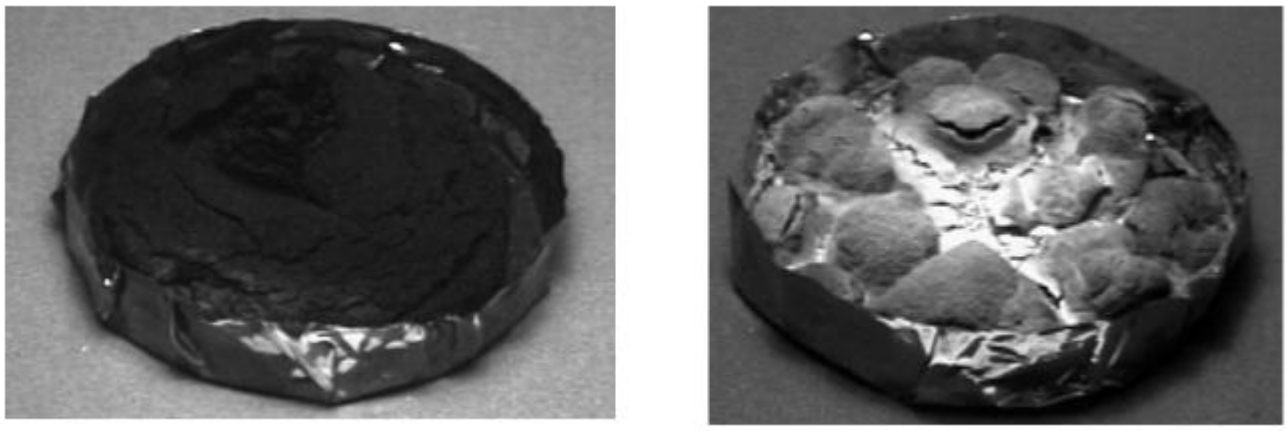

Figure 32. Digital photos of gasification residues from EVA/5 % MMT (SCPX 2156) (left) and EVA/5 % MMT (1.30D) (right).

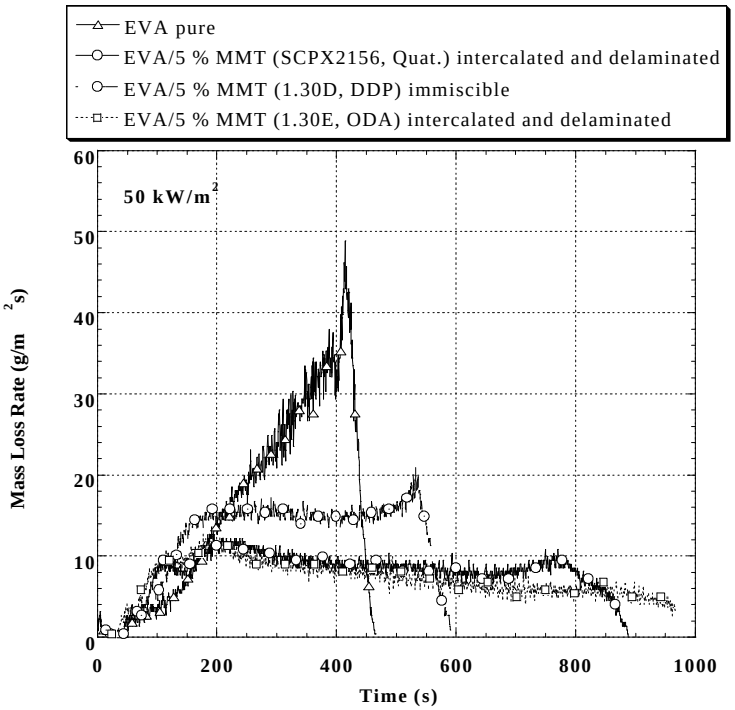

Figure 33. Mass Loss Rate data (flux: 50 kW/m^2) for pure EVA, and EVA/MMT samples with SCPX2156 (quaternary-MMT) or 1.30D (DDP-MMT) or 1.30E (ODA-MMT), non-irradiated samples.

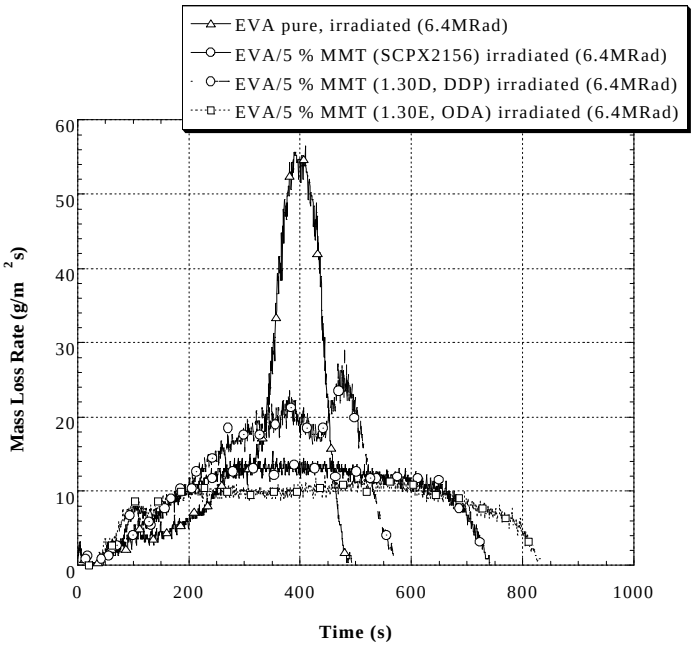

Figure 34. Mass Loss Rate data (flux: 50 kW/m^2) for pure irradiated-EVA, and irradiated-EVA/MMT samples with SCPX2156 (quaternary-MMT) or 1.30D (DDP-MMT) or 1.30E (ODA-MMT). All samples were irradiated at 64 kGy (6.4 MRad).

3.4.5. UL94 testing[10]

As we observed in the other nanocomposites, the burn to clamp times (BTC) can be longer but no self-extinguishing behavior is seen with any of the samples The data is shown in Table 24. Irradiated EVA samples were not tested.

Table 24. UL-94 burn data for EVA/MMT nanocomposites.

Sample	Avg. t_1(s)	Comments	t_2(s)	Comments
EVA/5 % MMT (SCPX2156)	66	BTC	-	-
EVA/10 % MMT (SCPX2156)	56	BTC	-	-
EVA/5 % MMT (1.30D, DDP)	47	BTC	-	-
EVA/5 % MMT (1.30E, ODA)	68	BTC	-	-

3.5. Epoxy nanocomposites

The focus for Year One for the epoxy nanocomposites was to look at tethered and non-tethered nanocomposites (critical experiment 2) and evaluate the effect of the type of clay (critical experiment 3) on the flammability properties. It was planned that a tether could be formed by reaction of the anhydride-curative with the alcohol group on the hydroxyethyl substituted quaternary alkyl ammonium treatment used on the MMT (SCPX 2003). The non-tethered samples were made using either the anhydride curative, or the aromatic amine curative and a non-reactive quaternary alkyl ammonium treatment on the MMT (SCPX 2165). Table 25 shows the samples prepared.

Table 25. Epoxy and Epoxy/MMT nanocomposite data.

Resin	Clay	Shear modulus	Glass transition temperature (T_g)	TGA inflection	XRD[a] spacing
Epoxy/ anhydride	none	1.45 GPa	125 °C	404 °C	-
Epoxy/ anhydride (non-tethered)	SCPX 2165	1.75 GPa	110 °C	396 °C	4.0 nm
Epoxy/ anhydride (tethered)	SCPX 2003	1.78 GPa	110 °C	394 °C	4.0 nm
Epoxy/ aromatic amine	none	1.24 GPa	168 °C	390 °C	-
Epoxy/ aromatic amine(non-tethered)	SCPX 2165	1.57 GPa	155 °C	376 °C	3.5 nm

a: XRD spacing was measured on the uncured resin mixture.
No XRD spacing was observed on any of the cured resin samples.

3.5.1. Characterization

The epoxy/MMT nanocomposites were characterized using XRD, TEM, thermal analysis (TGA), and mechanical analysis. The data are shown in Table 25. The XRD data, taken prior to cure of the epoxy/MMT nanocomposites, show they are intercalated. Since the XRD peaks all disappear after cure, these samples are disordered nanocomposites, thus requiring characterization by TEM. The epoxy/anhydride /MMT(tethered) (SCPX2003) nanocomposite contains intercalated intact tactoids with few delaminated MMT layers. The epoxy/anhydride/MMT(non-tethered) (SCPX2165) nanocomposite also appears to have intact tactoids, but the layer spacings may be larger than the tethered sample, and there are some delaminated, low aspect-ratio, MMT plates. These results are different from those reported by others on epoxy nanocomposites. Previous work (which used different curing agents) showed the necessity of intra-gallery reaction to assist in delaminating the layers[22]. Here the epoxy/anhydride /MMT(tethered) (SCPX2003) nanocomposite, which has a reactive MMT

treatment (hydroxyethyl), has an intercalated structure (Figure 35), but the two other epoxy nanocomposites, which have non-reactive MMT treatments, have apparently larger d-spacings and even some delaminated layers (Figure 36 and Figure 37).

Figure 35. TEM of epoxy/anhydride /MMT(tethered) (SCPX2003) nanocomposite.

Figure 36.TEM of epoxy/anhydride/MMT(non-tethered) (SCPX2165) nanocomposite.

Figure 37. TEM of epoxy/aromatic amine/MMT(non-tethered) (SCPX2165) nanocomposite.

The thermal (TGA, T_g) and mechanical characterization (shear modulus) of the epoxy/MMT nanocomposite are shown in Table 25. Although there is an improvement in the shear modulus, the thermal properties of the nanocomposites were not improved. The T_g are 10 °C to 15 °C lower than the neat epoxies, and the thermal stabilities are 10 °C to 20 °C lower.

3.5.2. Cone Calorimetry

The HRR data for the epoxy/aromatic amine control sample, and the epoxy/aromatic amine/MMT (non-tethered) (SCPX2165) nanocomposite are shown in Figure 38. Although, from the TEM (Figure 37) the nano-dispersion appears very good for this nanocomposite, the peak HRR is about the same as the control sample, and the HRR early in the burn is significantly higher. In contrast we see slightly lower peak HRRs for the epoxy/anhydride/MMT nanocomposites (Figure 39). However, early in the burn, these samples also show higher HRRs than the control. This may be caused by the same factors that give shorter t_{ign} and higher HRR early in both Cone and gasification experiments we observed in some of the other nanocomposites systems. However, the lower thermal stabilities seen in the TGA data may be responsible for the overall loss of effectiveness in the epoxies.

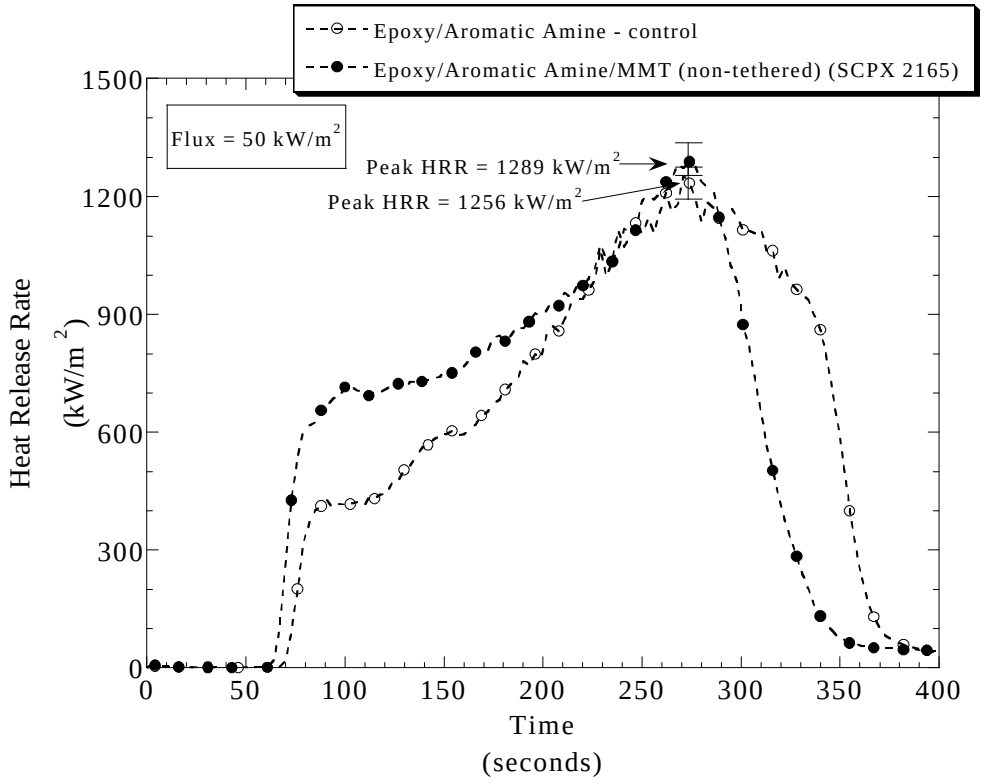

Figure 38. HRR data for epoxy/aromatic amine control sample and epoxy/aromatic amine/MMT(non-tethered) (SCPX2165) nanocomposite.

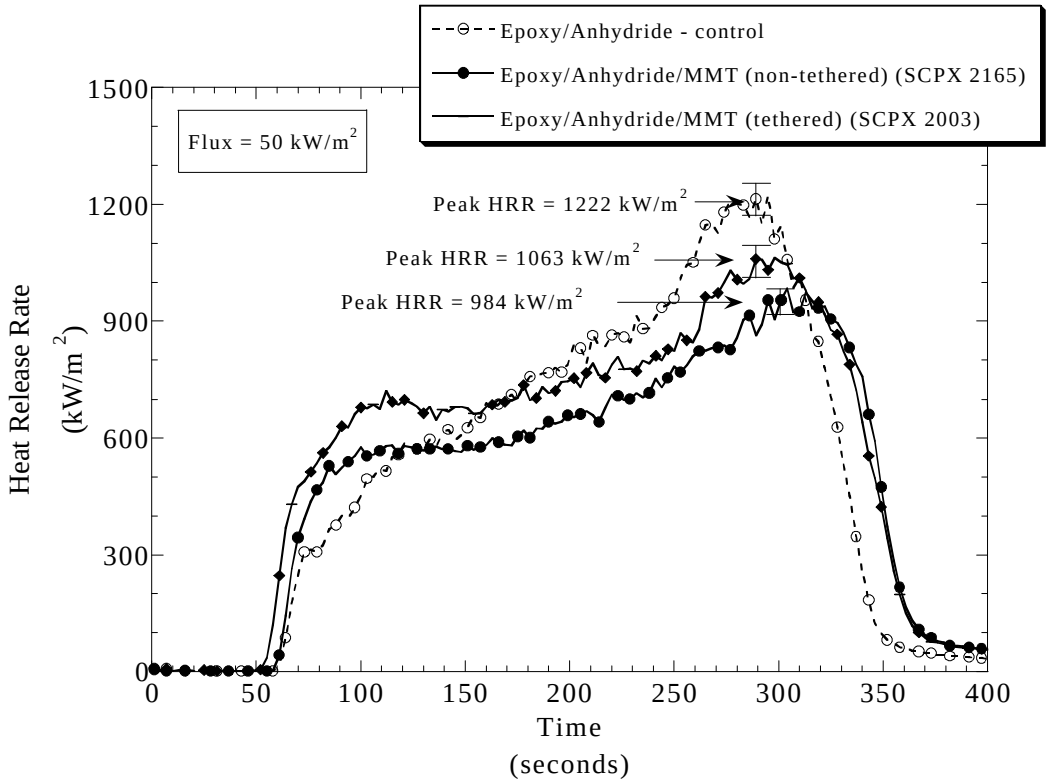

Figure 39. HRR data for epoxy/anhydride control sample, epoxy/anhydride/MMT(non-tethered) (SCPX2165) nanocomposite, and epoxy/anhydride/MMT(tethered) (SCPX2003) nanocomposite.

Nanocor has recently prepared epoxy nanocomposites using an aliphatic amine curing agent (Jeffamine D230) and ODA treated MMT (Nanomer 1.30E). The control sample had a peak HRR of 1313 kW/m^2 while the nanocomposite had a peak HRR of 1042 kW/m^2. This 20 % lower peak HRR is similar to that found for the epoxy/anhydride/MMT (non-tethered) (SCPX2165) nanocomposite.

These results are not only lower than expected, as compared to the other nanocomposites in this study, but also compared to preliminary results published previously, where a 40 % reduction in HRR was observed for an epoxy nanocomposite.[23] This epoxy was also a DEGBA epoxy, but was cured with methylenedianiline (MDA). In contrast to the 3M nanocomposite samples, which became disordered upon cure, the DEGBA/MDA/MMT nanocomposite remained ordered i.e., had an XRD peak and were therefore intercalated nanocomposites. Since the epoxy/aromatic amine/MMT (non-tethered) (SCPX2165) nanocomposite also appears to have an intercalated nanomorphology, it is not likely that the different nanomorphology is the cause of the different behavior.

3.5.3. Gasification

The video of the gasification experiment also reveals another possible source of the poor performance of these samples. In all of the other nanocomposite systems we have studied, we see formation of clay-reinforced carbonaceous char; we do not see formation of this type of char for these epoxy samples. Instead, the sample becomes a dark rapidly-boiling tar during gasification.

To determine the reason for the poor performance of the epoxy nanocomposites, additional work needs to be done. A check of the crosslink densities should be done, and the effect of the type of cure, clay treatment, and the effect of capping the SiOH and AlOH groups on the edge of the MMT plates should be investigated. The performance may also be improved by use of a co-additive.

4. Conclusions

The results from the first year are summarized in Table 26. The observed reductions in HRR are quite significant.[24] Other than the greatly reduced HRR, the most important result from our first year's work is the formation of a clay-reinforced carbonaceous char during combustion of nanocomposites. This is particularly significant for systems whose base resin normally produces little or no char when burned alone (PS, PPgMA, PA-6, and EVA). It appears from the gasification data (videos and mass loss data) that this clay-reinforced carbonaceous char is responsible for the reduced mass loss rates and hence the lower HRRs. Initially higher HRR and shorter t_{ign} are observed in many of the nanocomposites, and the origin of this effect needs to be better understood.

During the first year our goals were to compare the flammability properties of 1) intercalated versus delaminated nanocomposites, 2) tethered versus non-tethered nanocomposites, 3) nanocomposites with different layered silicates (clays), i.e., hectorite versus montmorillonite, 4) nanocomposites crosslinked to different degrees, 5) nanocomposites with different melt viscosities, 6) nanocomposites with different silicate loading levels and 7) nanocomposites incorporating a charring-resin, polyphenyleneoxide (PPO), into a blend.

We conclude that intercalated nanocomposites perform as well as delaminated nanocomposites. We were not able to determine if there is an effect of tethering, due to the weak overall effect observed for the epoxy nanocomposites in general. We did not explore nanocomposites with different layered silicates (clays), i.e., hectorite versus montmorillonite. We conclude that a small but significant effect on the lower HRR may be due to the greater melt viscosity of the nanocomposites, but rheological measurements still need to be made to confirm this conclusion. In terms of the effect of loading level, the effectiveness of the nanocomposite approach to reducing HRR, in most cases, levels off at 5 % silicate loading. And finally, the use of a char-enhancer (PPO) did not decrease the flammability of the PA-6 nanocomposites, but other char-enhancing co-additives should be explored.

Summaries of the Cone Calorimeter data for each of the polymer resins + 5 % clay is included in Tables 28 to 32.

Table 26. Summary of results.

Result/Critical Experiment	EVA	PA-6	PS	Epoxy	PP
Peak HRR reduced	70 %	80 %	80 %	0 - 20 %	70 %
Shorter t_{ign}	no	yes	no	no	no
High initial HRR or MLR	yes	no	yes	yes	yes
Carbonaceous char formed	yes	yes	yes	no	yes
Intercalated vs. delaminated	-	equivalent	-	-	-
Tethered vs. non-tethered	-	-	-	-	-
Effect of different clays	-	-	-	-	-
Effect of crosslinking	TBD	-	-	-	-
Effect of Mw	-	-	moderate	-	-
Effect of loading level	5 % max	10 % max	5 % max	TBD	5 % max
Effect of charring resin (PPO)	-	none	-	-	-

Table 27. Cone Calorimeter Data Summary for Nylon-6 / 5 % MMT Samples.

	Residue Yield [%]	Peak HRR [kW/m^2]	Specific Ext. Area [m^2/kg]	H_C [MJ/kg]	Peak MLR (cone) [g/s]	Peak MLR (Gas.) [g/s]	Clay Treatment (d-Spacing)	Company Sample Number
Nylon-6	0.81 %	2105	197.44	36.4	56.53	40.50		-
5 % MMT (in situ)	5.15 %	801	337.94	33.0	23.28	19.01		-
5 % MMT (delaminated)	3.94 %	737	325.37	33.1	21.65	19.01	Quaternary, (2.45 nm)	021899-2
5 % PPO/ 4.752 % MMT (delaminated)	4.83 %	664	386.37	31.8	20.72	15.84	Quaternary, (2.45 nm)	021899-4

Uncertainties for this data can be found in the original Cone Calorimeter Plots – Figures 4 and 6.

Table 28. Cone Calorimeter Data Summary for Polypropylene / 5 % MMT Samples.

	Residue Yield [%]	Peak HRR [kW/m^2]	Specific Ext. Area [m^2/kg]	H_C [MJ/kg]	Peak MLR (cone) [g/s]	Peak MLR (Gas.) [g/s]	Clay Treatment (d-Spacing)	Company Sample Number
Polypropylene	0.00 %	2440	668.58	44.7	51.35	39.819	-	#1
15 % PP-g-MA	0.22 %	3020	721.70	49.1	57.98	42.081	-	#2
5 % MMT (intercalated (2.63 nm))	3.18 %	934	1001.86	46.4	19.63	18.552	Quaternary, (2.54 nm)	#3
5 % MMT/ 15 % PP-g-MA (intercalated (3.62 nm) and delaminated)	3.63 %	766	1070.99	45.5	16.57	18.552	Quaternary, (2.54 nm)	#4
5 % MMT (intercalated (2.70 nm))	3.74 %	1139	964.11	46.9	23.68	18.552	ODA Primary, (2.20 nm)	#7
5 % MMT/ 15 % PP-g-MA (intercalated (3.56 nm) and delaminated)	4.53 %	740	1057.62	46.2	16.00	14.48	ODA Primary, (2.20 nm)	#8

Uncertainties for the data can be found in the original Cone Calorimeter Plots – Figures 22 and 23.

Table 29. Cone Calorimeter Data Summary for Epoxy / 5 % MMT Samples.

	Residue Yield [%]	Peak HRR [kW/m^2]	Specific Ext. Area [m^2/kg]	H_C [MJ/kg]	Peak MLR (cone) [g/s]	Peak MLR (Gas.) [g/s]	Clay Treatment (d-Spacing)	Company Sample Number
Epoxy Resin								
Anhydride Cured/ 5 % MMT (intercalated)	10.89 %	974	973.02	23.6	41.31	34.602	OH-Quat. (2.44 nm) & (1.82 nm)	112545-97
Aromatic Amine Cured/ 5 % MMT (intercalated)	11.84 %	1309	1421.01	27.1	47.55	42.215	Quaternary, (1.75 nm)	112545-98
Anhydride Cured/ 5 % MMT (intercalated)	9.76 %	1263	1043.91	25.6	49.30	34.602	NH2 Quaternary, (1.25 nm)	112545-99
Anhydride Cured Control	4.01 %	1235	1009.04	23.3	52.43	32.872		112545-100
Aromatic Amine Cured Control	4.56 %	1297	1374.21	24.4	51.95	43.945		112545-101
Cured (intercalated)	10.10 %	1069	957.42	25.5	43.47	-		112545-102

Uncertainties for the data can be found in the original Cone Calorimeter Plots – Figures 38 and 39.

Table 30. Cone Calorimeter Data Summary for Polystyrene / 5 % MMT Samples.

	Residue Yield [%]	Peak HRR [kW/m^2]	Specific Ext. Area [m^2/kg]	H_C [MJ/kg]	Peak MLR (cone) [g/s]	Peak MLR (Gas.) [g/s]	Clay Treatment (d-Spacing)	Company Sample Number
Polystyrene (High MW)	0.21 %	1873	1323.12	31	59.25	40.724		Styron 663
5 % MMT (intercalated (3.27 nm) and delaminated))	4.88 %	545	1232.65	26	21.81	14.027	Quaternary, (2.42 nm)	3981-84-5
Polystyrene (Low MW)	0.26 %	1942	1299.23	31	63.40	41.629		XU 70262.08
5 % MMT (intercalated (3.34 nm) and delaminated))	4.87 %	544	1648.19	29	19.43	12.670	Quaternary, (2.42 nm)	3981-84-2

Uncertainties for the data can be found in the original Cone Calorimeter Plots – Figures 17 and 18.

Table 31. Cone Calorimeter Data Summary for Polyethylene-co-Vinyl Acetate / 5 % MMT Samples.

	Residue Yield [%]	Peak HRR [kW/m^2]	Specific Ext. Area [m^2/kg]	H_C [MJ/kg]	Peak MLR (cone) [g/s]	Peak MLR (Gas.) [g/s]	Clay Treatment (d-Spacing)	Company Sample Number
Ethylene Vinyl Acetate	0.00 %	1850	524.39	38	43.63	48.869	-	17613-31-1
5 % MMT	5.22 %	613	897.58	36.0	17.60	12.670	ODA Primary, (2.20 nm)	17613-35-2
5 % DDP	3.16 %	1098	620.61	40	26.82	21.267		17613-35-4
5 % MMT (intercalated, (4.25 nm))	4.98 %	564	860.02	35	16.71	12.670	Quaternary, (2.42 nm)	17613-34-5

Uncertainties for the data can be found in the original Cone Calorimeter Plots – Figures 31 and 33.

REFERENCES

[1] Gilman, J. W., Kashiwagi, T., Lichtenhan, J. D., *SAMPE Journal*, **1997,** vol. 33, no. 4, 40.

[2] Giannelis, E., Advanced Materials, **1996**, 8, 29.

[3] Fujiwara, S., Sakamoto, T., Kokai Patent Application, no. SHO 51(1976)-109998, **1976.**

[4] Usuki, A., Kojima, Y., Kawasumi, M., Okada, A., Fukushima, Y., Kurauchi, T. and Kamigaito, O., J. Mater. Res. **1993**, 8, 1179.

[5] According to ISO 31-8, the term "Molecular Weight" has been replaced by "Relative Molecular Mass", symbol M_r . Thus, if this nomenclature and notation were used here, $M_{r,n}$ instead of the historically conventional *Mw* for the average molecular weight (with similar notation for M_w, M_z, M_v) would be used. It would be called the "Number Average Relative Molecular Mass". The conventional notation, rather than the ISO notation, has been employed here.

[6] Morgan, A. B.; Gilman, J. W.; Jackson, C. L. *Polym. Mater. Sci. Eng.*, **2000**, *82*, 270.

[7] Babrauskas, V., Fire and Materials, **1995**, 19, 243.

[8] The Cone data for pure PA-6 shown in the HRR and MLR plots is for the material from UBE. However the PA-6 used by GE to prepare the nanocomposites (from Allied Signal) has very similar flammability properties to the UBE material.

[9] Gilman, J. W.; Kashiwagi, T.; Lichtenhan, J. D. *SAMPE Journal* **1997**, *33* **,** 40.

[10] Underwriters Laboratories UL 94: Standard for Tests for Flammability of Plastic Materials for Parts in Devices and Appliances., 4th Ed. Research Triangle Park, NC, Underwriters Laboratories, Inc., 1991. The UL-94 test is a qualitative pass/fail test, and while it provides quantities (burn times), the data from this test cannot be held up to a strict error analysis.

[11] Gilman, J.; Kashiwagi, T.; Lomakin, S.; Giannelis, E.; Manias, E.; Lichtenhan, J.; Jones, P. in Fire Retardancy of Polymers : the Use of Intumescence. The Royal Society of Chemistry, Cambridge, 1998, 203-221.

[12] TGA data were collected on a TA Instruments model# 2950 under N_2 at 10 °C/min from 30 °C to 700 °C.

[13] Conventional gel permeation chromatography (GPC) was carried out on a Waters Alliance 2690 equipped with a Viscotek LR40 Laser Refractometer. The column set consisted of four 300 x 7.5mm PLGel 5 micron columns (1000 nm, 100 nm, 50 nm, and 10 nm) in series. The mobile phase was THF at a flow rate of 1 mL/min. The calibration curve was set up using narrow polystyrene standards, available from American Polymer Standards, with the following molecular weights: (675000, 350000, 212000, 115000, 30300, 17000, 9000, 3600, 2100, and 162 g/mol). Samples and standards were prepped in THF at 2mg/mL.

[14] Gilman, J., Manias, V., Jackson, C., Morgan, A., and Harris, R., Jr, *Chem Mater.* In press.

[15] This assumes $\eta \sim Mw^{0.6\text{-}0.8}$ see Textbook of Polymer Science, ed. Billmeyer, F. John Wiley & Sons, New York, 1984, 211.

[16] Bourbigot, S., LeBras, M., Dabrowski, Gilman, J., and Kashiwagi, T. Proceedings of 10th BCC Annual Conference, May 1999.

[17] Inoue, H.; Hosokawa, T., 1998 Japan Patent (Showa Denko K. K., Japan) Jpn. Kokai tokkyo koho JP 10 81,510 (98 81,510).

[18] Takekoshi et al., Fire Retardant Blends, US patent 5,773,502 (1998, GE Company).

[19] Klatt et al., Flameproof Thermoplastic Molding Materials, PCT Int. Appl. WO98 36,022 (1998, BASF AG)

[20] Nyden, M. R.; Forney, G. P.; Brown, J. E. *Macromolecules* **1992**, *25*, 1658.

[21] Nyden, M. R.; Brown, J. E. *NISTIR 5509* October 1994.

[22] (a) Wang, M. S.; Pinnavaia, T. J. Chem. Mater. 1994, 6, 468. (b) Messersmith, P. B., Giannelis, E. P., Chem. Mater.1994, 6, 1719.

[23] Gilman, J. W., Kashiwagi, T., Nyden, M., Brown, J. E. T., Jackson, C. L., Lomakin, S., Giannelis, E. P., Manias, E., in Additives and Modifiers for Polymers A. Golovoy, S. Al-Malaika, C. Wilkie eds., Blackwell Science, London (1999) pp. 249-265.

[24] The uncertainty analysis of these results shows that the HRR reductions are not only large, but are real numbers. Specifically, the reduced peak HRR numbers are not just a result that falls within a combined uncertainty. There are several possible areas for uncertainty, including the exact amount of clay and additive loading, sample irregularities, and Cone calorimeter data. While we do not know the combined uncertainty from all of these factors, we are able to comment on each of them. We are unsure about the exact amount of clay or additive loading in these samples, but given the HRRs observed at stated loadings, we believe that the observed effects are real, and not just a fluke result associated with a clay loading. (i.e., ± 2 % of the stated clay loading) We believe the samples to only have small irregularities, as characterization of these samples by TEM and XRD showed them to be homogenous and the type of nanodispersion of the clay was characterized. The Cone calorimeter data at 50 kW/m^2 has been shown to be reproducible to within ± 10 %. Given this, we feel confident that the significant reduction in HRR for these samples is a true result, and it makes the flame reduction effect that much more impressive. See also refs. 1, 14, and 23.